Annu. Rev. Nucl. Part. Sci. 1997. 47:67–109

SOLID POLARIZED TARGETS FOR NUCLEAR AND PARTICLE PHYSICS EXPERIMENTS

D. G. Crabb
Physics Department, University of Virginia, Charlottesville, Virginia 22901

W. Meyer
Institut für Experimentalphysik I, Ruhr-Universität Bochum, Bochum, Germany

KEY WORDS: dynamic polarization, nucleon spin structure, lepton scattering, cryogenics, asymmetry

ABSTRACT

The development, in the early 1960s, of the dynamic nuclear polarization process in solid diamagnetic materials, doped with paramagnetic radicals, led to the use of solid polarized targets in numerous nuclear and particle physics experiments. Since then steady progress has been made in all contributing subsystems so that proton polarizations near 100% and deuteron polarizations higher than 50% have been achieved in various materials. More radiation-resistant materials, such as ammonia, have made it possible to perform experiments with high beam intensities and experiments that benefit from ^{4}He cooling at 1K and high magnetic fields. The development of dilution refrigerators have allowed frozen spin operation so that experiments with large angular acceptance for the scattered particles have become routine. Many experiments have taken advantage of these developments and many more are being planned, especially with electromagnetic probes.

CONTENTS

0163-8998/97/1201-0067$08.00

1. INTRODUCTION

The advent of solid polarized targets in the early 1960s opened up a new era in the study of particle interactions. The first experiment with a polarized target was at Saclay (1), at low energy, and soon was followed by a high-energy experiment at the Lawrence Radiation Laboratory Berkeley (2) and a rapid expansion in the use of such targets at most laboratories in the world. The availability of the polarized proton and, then, deuteron (neutron) targets, whose spin could be oriented in any direction, allowed the detailed study of hadron-hadron interactions. In interactions with spinless particles, such as π and K-mesons, the spin-sensitive part could be extracted and used to discriminate among various theories. Together with polarized nucleon beams it became possible to study extensively the nucleon-nucleon interaction. The motivation of this research program, which was mainly at lower energy laboratories such as the Japanese National Laboratory (KEK), Los Alamos Meson Physics Facility (LAMPF), the Swiss National Laboratory (SIN, now PSI), Saclay, and Argonne National Laboratory (ZGS), as well as at higher energies at CERN, was to probe and extend our knowledge of the specific details of spin dependencies of the various interactions and to check the theoretical models invoked to explain them.

Meanwhile there was less progress using polarized targets with electrons, due to limitations in technology and the limited gain in understanding of the underlying physics processes that polarizing only the nucleon could provide. However, at the Stanford Linear Accelerator Center (SLAC), development of a polarized electron beam meant that new regions of physics could be probed and, for the first time, an attempt could be made to use deep inelastic scattering (DIS) to measure the spin content of the proton carried by the quarks (3, 4).

At the same time, however, polarized proton and deuteron (neutron) targets were operated at the University of Bonn, the UK Laboratory for Nuclear Science, Daresbury, DESY, Kharkov in Ukraine, and Tokyo (INS) to measure polarization observables with real (polarized) photon beams to improve the knowledge about the electromagnetic properties of baryon resonances.

Since 1962, the many technical developments in target materials, refrigerators, magnets, and associated equipment have meant that present-day targets can have high polarization, oriented in any specified direction, high polarizable nucleon content and resistance to radiation damage. These developments have made it possible to access progressively lower cross section interactions with better precision. This is highlighted in the measurements of the analyzing power A_N in proton-proton elastic scattering from 24 - 28 GeV/c. The first measurements at the PS at CERN (5) were made with limited beam intensity and propanediol as the target material. Radiation damage of the propanediol and limitations in the cooling of the target material restricted the beam intensity that could be used and, therefore, compromised the statistical precision for scattering at high $P_\perp^2$. The next experiment at the Brookhaven National Laboratory, AGS, (6) had improved ^{3}He refrigeration and used ammonia as the target material. This combination allowed a beam intensity of approximately a factor of 10 higher to be used and, therefore, led to improved precision on the measurements and the extension to higher $P_\perp^2$. A second experiment at the AGS (7) was able, with a new ^{4}He evaporation refrigerator and magnet system (8) and with ammonia still as the target material, to increase the usable beam intensity by another factor of 10 and further reduce statistical errors and extend the $P_\perp^2$ range. This is summarized in Figure 1.

These experiments and others show how the emphasis shifted from the low $P_\perp^2$ Regge region to high $P_\perp^2$ where Perturbative Quantum Chromodynamics (PQCD) effects could be investigated. A wealth of data have emerged from these polarization experiments, but to a large extent remain unexplained. An example is that of the measurement of A_{NN} at 90° center of mass scattering in proton-proton elastic scattering (9). Despite many attempts these data have not been satisfactorily explained and, paradoxically, there appears to have been a lessening of theoretical interest in polarized hadron-hadron scattering, coupled with a decline in the facilities for performing these experiments.

The decline in experiments with polarized targets and hadron beams has been paralleled by a surge of activity at electron machines. The Standard Model, the strong interaction theory of quantum chromodynamics (QCD), tells that the valence quarks and the sea quarks are spin-1/2 objects bound by gluons which are spin-1 objects. The presence of particles with spin inside the hadrons has moved the question of spin phenomena to the forefront; at SLAC and at CERN, the most advanced polarized solid state targets are installed in an electron and

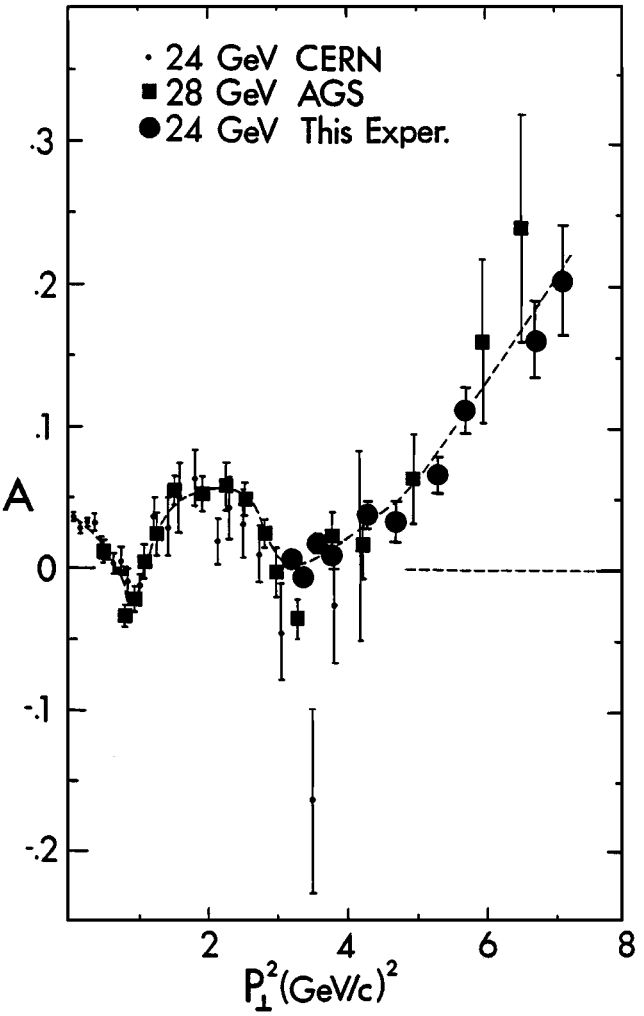

Figure 1 The analyzing power, *A*, in proton-proton elastic scattering, as a function of momentum transfer squared, $P_{\perp}^2$, from three experiments; at 24 GeV/c at the CERN PS [Ref. 5], 28 GeV/c at the Brookhaven AGS [Ref. 6] and at 24 GeV/c at the AGS [Ref. 7].

muon beam, respectively, for deep inelastic measurements of the spin structure of the nucleon.

However, especially in the non-pertubative energy range, the understanding of the saturation of the color forces is incomplete. In this regime of up to several GeV, a rich program is in progress at the new continuous beam facilities at Bonn, the University of Mainz, MIT-Bates, NIKHEF, and Thomas Jefferson National Accelerator Facility (TJNAF, formerly CEBAF). They all have improved equipment for studying spin effects extensively: polarized targets, polarized electron- and γ-beams and polarimeters combined with improved detector set-ups. The first polarized target experiments, using a brand new frozen-spin refrigerator, have already been performed with a tagged photon beam facility at the electron stretcher accelerator ELSA in Bonn (10). Clearly in the next few years there will be a host of new measurements that should greatly improve our understanding of the structure of nucleons and nuclei.

In this review we discuss the principles of dynamic nuclear polarization. In Section 3, we describe the major pieces of equipment necessary to realize an operational polarized target. The frozen-spin target technique is described in Section 4. In Section 5, we discuss examples of state-of-the-art targets in the context of the experimental programs at various laboratories.

2. POLARIZATION MECHANISMS

The method of dynamic nuclear polarization (DNP) described in this review was developed in 1953 for metals (Overhauser effect) (11) and in 1958 for solid insulators (solid state effect) (12–14). The basic idea—to obtain a high polarization $P_I = < I_Z > / I$ of nuclear spins—consists of using a microwave field, in a high magnetic field, to transfer the polarization $P_S = < S_Z > / S \approx -1$ of electron spins to these nuclei. The following description of the DNP process is restricted to polarized nucleon targets, i.e. proton and deuteron (neutron), that have been used in numerous nuclear and particle physics experiments during the last three decades. These polarization mechanisms, though, are also valid for polarized nuclei. The main problem with DNP is finding a suitable combination of hydrogen- or deuterium-rich material and a paramagnetic dopant, i.e. material with an unpaired or quasi-free electron. Suitable means that the relaxation time of the electron spins is short (ms) and that of the nucleons is long (min). Molecular hydrogen would be the ideal proton target material, except that at low temperature it devolves to the magnetically inert para-state, with spin zero and, hence, is unpolarizable. However, various practical polarized target materials have been developed in which the paramagnetic centers have been introduced by chemical or radiation methods (see Section 3.5). Since the electron line width is another dominant factor for DNP, there are different DNP

schemes. In this section, we start with the description of thermal equilibrium polarization and describe the most important DNP principles, i.e. the solid-state effect (SSE), and the equal spin temperature (EST) theory. Finally we compare the polarization mechanisms.

2.1 *Thermal Equilibrium Polarization*

The starting-point of any general discussion of polarized targets is the magnetic moment of each of the particles of interest, i.e. the electron and proton or deuteron. A polarized target can be assumed to be an ensemble of such particles placed in a high magnetic field and cooled to low temperature. The Zeeman interaction between the magnetic moment μ and the external magnetic field B establishes a set of $2I + 1$ sublevels, where the spin $I = 1/2$ is valid for protons and $I = 1$ for deuterons. At thermal equilibrium the population of two magnetic sublevels is described by the Boltzmann law

$$N_1 = N_2 \cdot \exp\left(\frac{-\Delta E}{k_B T}\right), \qquad 1.$$

where T is the temperature of the system, k_B is the Boltzmann constant, and $N_{1,2}$ are the corresponding population numbers of the magnetic sublevels (Figure 2). In using the definition of the polarization of a spin-1/2 system by $P(1/2) = (N_{1/2} - N_{-1/2})/(N_{1/2} + N_{-1/2})$ and the vector polarization of a spin-1 system by $P(1) = (N_1 - N_{-1})/(N_1 + N_0 + N_{-1})$, the thermal equilibrium polarization is described by

$$P(1/2) = \tanh\left(\frac{g_i \mu_i B}{2k_B T}\right); \qquad P(1) = \frac{4\tanh\left(\frac{g_i \mu_i B}{2k_B T}\right)}{3 + \tanh^2\left(\frac{g_i \mu_i B}{2k_B T}\right)}. \qquad 2.$$

Unfortunately, the magnetic moment of the proton μ_p is small and that of the deuteron is even smaller. As a consequence, the nucleon polarization obtained in this way is very small. In a magnetic field of 2.5 Tesla and at a temperature of 1 K, a polarization of only 0.25% for protons and 0.05% for deuterons is obtained. However, electrons with their much higher magnetic moment ($\mu_e = 660\mu_p$) are highly polarized (92% at 2.5 T and 1 K). Of course, these nucleon polarization values are not very useful for nuclear and particle physics experiments. The technique of DNP, however, allows very high nucleon polarizations to be obtained.

2.2 *Solid-State Effect*

A very simplified description of the solid-state effect can be given as follows: A suitable solid target material with a high concentration of polarizable nucleons is doped with paramagnetic radicals which provide unpaired electron spins.

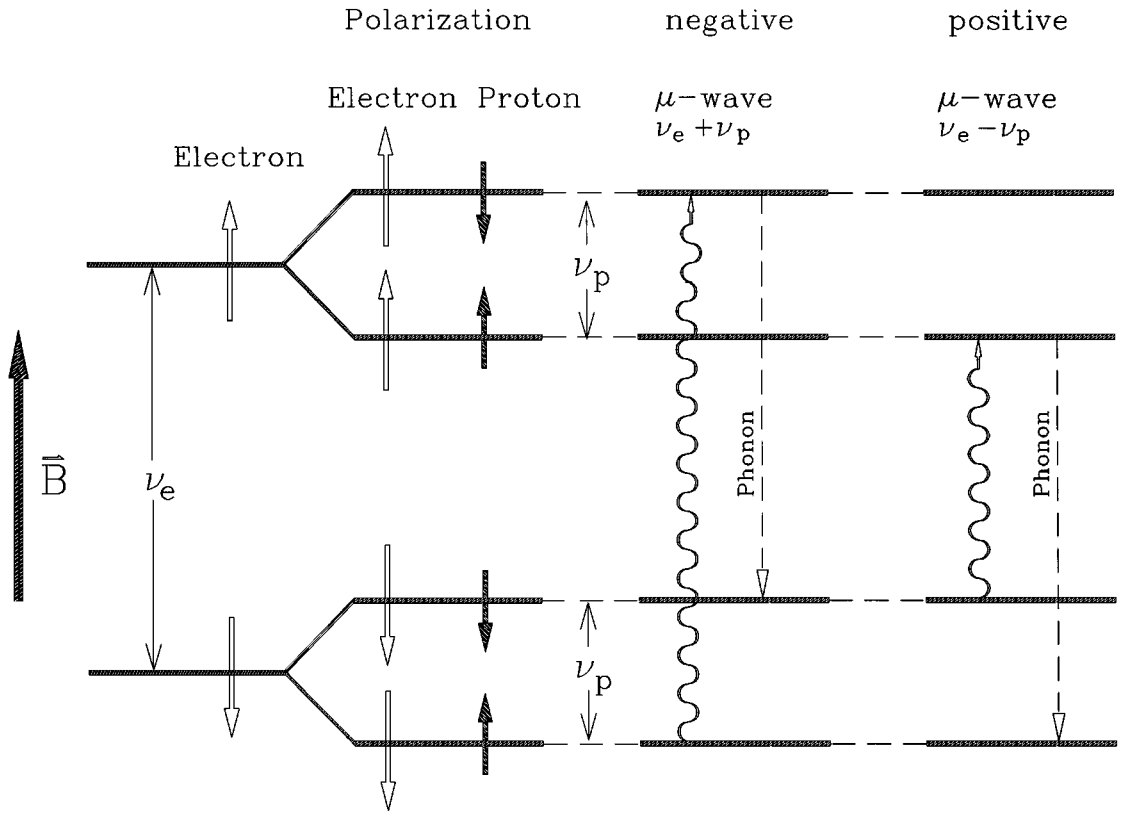

Figure 2 Schematic demonstration of the resolved solid-state effect.

As the magnetic moment of the electron is very much larger than that of the nucleon, the electron polarization is very high. The dipole-dipole interaction between the nucleon and electron spins leads to hyperfine splitting, which provides the contact between both spin species. By applying a suitable RF-field with a frequency very close to the electron spin resonance frequency—about 70 GHz at 2.5 T—the high electron polarization can be transferred to the proton. DNP works because the relaxation time for the nucleon spins is much longer than for the electron spins. The nucleon polarization can be directed either parallel or antiparallel to the applied magnetic field by using slightly different values for the frequency (Figure 2). No other parameter that can influence the experiment needs to be changed. This is a very important feature of the DNP, as systematic errors are reduced to a very low level.

In a theoretical description of the solid-state effect, one can give a quantum mechanical description of it using a Hamiltonian containing the Zeeman interactions of the nucleon spins and the electron spins only. Because this Hamiltonian has discrete levels, the time development of the system, due to a perturbation such as a microwave field or spin-lattice relaxation, can be reduced to rate equations (15). These are linear equations giving the time dependence of the probability of finding the system in a certain state. In this model, it is assumed that only one of the forbidden transitions ($\nu_e \pm \nu_n$) is excited. This is valid if the electron spin resonance (ESR) spectrum of the paramagnetic radicals is narrow compared to ν_n. The population numbers of the dynamic equilibrium essentially depend on the line width $\Delta\nu_e$, on the relaxation times of the electrons and the electron-nucleon coupling. These values determine the range of temperature and magnetic field in which dynamic polarization is feasible. In addition, the maximum polarization depends on microwave intensity. Relaxation processes are a limiting factor due mainly to paramagnetic impurities, i.e. such radicals that do not contribute to the build-up of nucleon polarization (see Section 3.7). The model of the solid-state effect describes very well the polarization mechanism in the first successful target material $La_2Mg_3(NO_3)_{12}* 24H_2O$ (LMN), a crystalline salt doped with neodymium, that provides the unpaired electron spins (1, 16).

2.3 *Equal Spin Temperature Theory*

In the present-day polarized target materials, such as frozen alcohols (chemically doped with free radicals) or ammonia and lithium compounds, in which the radicals are introduced by irradiation (see Section 3.5), the process of dynamic polarization is somewhat different from the simple scheme of the solid-state effect and is described by the theory of equal spin temperature (EST). Spin temperature models become important in those cases where the concentration of the electrons is so high that dipolar interactions of the electron spins cannot

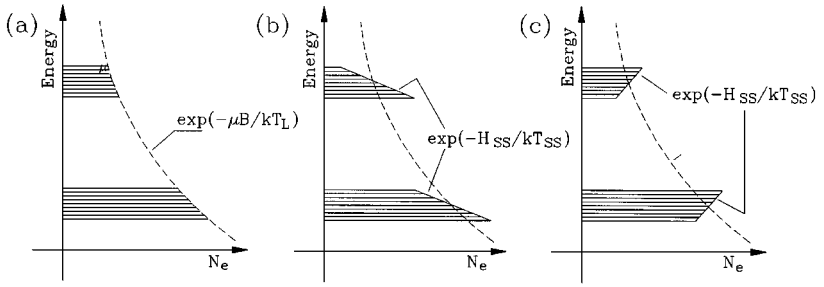

Figure 3 Population densities of the electron levels N_e at different temperatures of the spin-spin interaction reservoir T_{SS} and electron Zeeman reservoir T_{Ze}. (*a*) Spin-spin interaction reservoir and Zeeman reservoir in thermal equilibrium with the lattice: $T_{SS} = T_{ZE} = T_L$, (*b*) $0 < T_{SS} < T_{Ze}$, (*c*) $T_{SS} < 0, 0 < |T_{SS}| < T_{Ze}$.

be neglected in the description. These interactions are weak in comparison to the Zeeman interaction of the electron spins. In this case, the energy levels are not discrete, i.e. there is no uniform energy level for equal spin quantum numbers but rather a band of quasi-continuous states. So it is extremely difficult to describe the time evolution of the system under the influence of a perturbation, such as a microwave field or spin lattice relaxation, by means of rate equations. The population of the states inside such a band, as well as the population of different bands, are described by a Boltzmann distribution with the temperatures T_{SS} and T_{Ze} being the temperatures of the electron spin-spin interaction reservoir (SSI-reservoir) and the electron Zeeman reservoir, respectively. Only in thermodynamic equilibrium, i.e. without microwave irradiation and after certain relaxation processes, are T_{SS} and T_{Ze} identical with the lattice temperature T_L (Figure 3*a*). The introduction of the temperature T_{SS} is necessary, as the spatial spin distribution by the spin-spin interaction provides an additional energy reservoir that, without relaxation processes, is independent of the Zeeman reservoir and the lattice temperature. In analogy to the heat reservoir of the lattice vibrations (phonons), the energy of this reservoir is characterized by a temperature, which can also have negative values (Figure 3*b*,*c*). This means that the population of the upper levels inside a band is higher than the population of the lower ones. A different T_{SS} at constant T_{Ze} means that on average the number of spins in the magnetic field direction is constant, but the spatial distribution is not.

DNP in this spin temperature concept proceeds in two steps:

1. Cooling of the electron SSI-reservoir. In the first step a quantum with the energy $h(\nu_e - \Delta)$ is absorbed from the microwave field. The energy is divided into two parts—one part $h\nu_e$ that is used to change the electron

Zeeman energy and one part $h\Delta$ that is absorbed by the electron SSI-reservoir. If $\Delta > 0$, this just means that the SSI-reservoir must emit this energy, and it cools down. If $\Delta < 0$, the SSI-reservoir is heated, and T_{SS} may become negative (Figure 3).

2. Heat contact between the electron SSI-reservoir and Zeeman-reservoir of the nucleons (thermal mixing). The second step is the proper thermal mixing process. For this a (forbidden) relaxation process is considered. It consists of a flip-flop of two electron spins together with a flip of nucleon spin. The energy of the electron-Zeeman-reservoir remains unchanged, whereas that of the nucleon-Zeeman-reservoir changes by $h\nu_n$. In this case, the energy conservation is guaranteed by the SSI-reservoir, as this relaxation mechanism should take place without participation of the lattice. In any such process, the energy $h\nu_n$ is exchanged between both reservoirs. As a consequence T_{SS} and T_{Zn} are equalized. By means of a further mechanism the microwaves can also contribute to this heat contact. The required frequency is close to the electron Larmor frequency also. A detailed description of these processes is given in (17). The development of the DNP theory in solid targets is described in review talks by A. Abragam (18) and C. D. Jeffries (19).

2.4 *Comparison of the Polarization Mechanisms*

In these different models that contain some immeasurable parameters, predictions of the absolute polarization values are not possible. Experimentally the above-mentioned polarization mechanisms can easily be distinguished if there are more than one spin species in the sample. If the solid-state effect is valid, the expectation is that the maximum polarization for the nuclei with the same spin but different magnetic moment are found at different microwave frequencies. In the ideal case, nuclear polarization can reach the polarization of the electrons. In the case of equal spin temperatures, the optimum frequency is only given by the cooling of the SSI-reservoir, i.e. optimum polarization for different nuclei can simultaneously be achieved at a unique microwave frequency. Then the polarization is determined by the common spin temperature T_{SS}, and depends only on the magnetic moment of the nucleus, e.g. for spin-1/2:

$$P(1/2) = \tanh\left(\frac{g_i \mu_i B}{2k_B T_{SS}}\right). \qquad 3.$$

As long as we are able to measure the polarization of one specific nucleus, all other polarizations in the material can be calculated via generalization of Equation 3 (Brillouin function). Hence, nuclei with a small magnetic moment are handicapped. Experimentally, this spin concept was first verified with samples of D-butanol and D-ethanediol, in which part of H-atoms were replaced

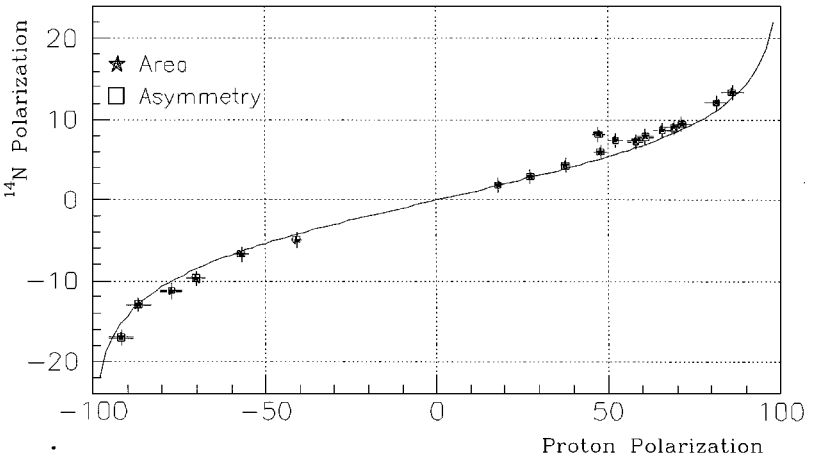

Figure 4 The figure shows the relation between the proton and the ^{14}N polarization in $^{14}NH_3$. The solid line corresponds to the EST prediction and the data points were measured with two different methods. They agree within the errorbars.

by D-atoms (20). The EST theory has since been experimentally confirmed in other materials. The most recent proof of this theory was with $^{14}NH_3$ (Figure 4), where the ^{14} N-H system shows equal spin temperatures during the DNP pumping process (21).

3. EQUIPMENT AND TECHNIQUES

Figure 5 shows a schematic of a generic polarized target, showing all the necessary subsystems. The polarizable material is cooled to a low temperature ($\leq$1 K), placed in a homogenous magnetic field of 2.5 T or greater and irradiated with microwaves. A nuclear magnetic resonance (NMR) system measures the degree of polarization. Not shown are the standard vacuum and pumping systems and instrumentation.

The first nuclear experiment (1) and (then) high-energy experiment (2) used lanthanum magnesium nitrate (LMN) doped with a rare earth radical such as neodymium and was cooled by a liquid ^{4}He evaporation refrigerator to $\approx$1 K. This material could be polarized to $\pm$ 70%. Despite the fact that there were only 3.1% of polarizable protons by weight, many experiments were done with LMN. With the discovery of high polarizations in organic materials, such as propanediol and butanol ($\approx$10% polarizeable protons) at CERN in 1968 (22), a new class of experiments could be started at various laboratories around the world. These materials required paramagnetic dopants such as Cr (V) or

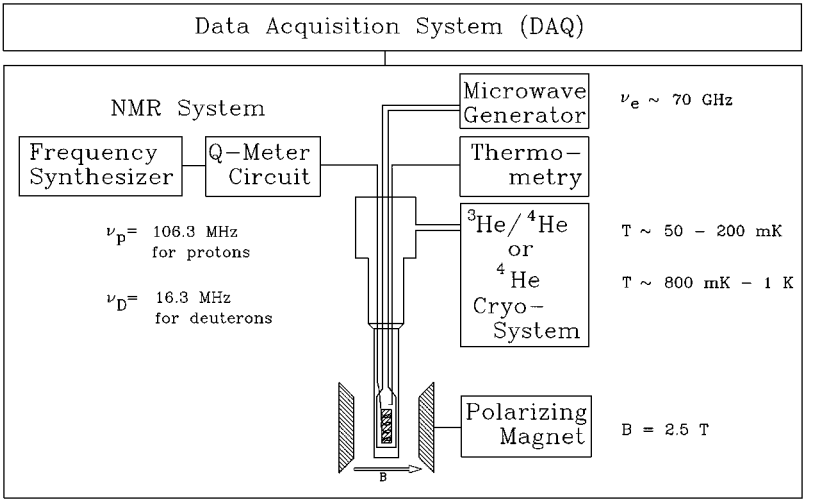

Figure 5 A generic polarized target showing the major subsystems and typical operational parameters. Not shown are the standard vacuum and Roots pumping systems.

porphyrexide and have a much higher polarization resistance against radiation damage compared to LMN.

A parallel development that also boosted achievable polarizations was the availability of ^{3}He. ^{3}He evaporation refrigerators started to be used and provided the ability to cool to ≈0.5 K rather than the 1 K possible with ^{4}He. Since the polarization is related to $\exp(-\frac{\mu B}{kT})$, the achievable polarization could, in fact, be doubled. This is shown in Figure 6, taken from deBoer & Niinikoski (23). However, the thermal properties of ^{3}He limit the amount of beam intensity that can be tolerated before the polarization is reduced to an unacceptable level.

Dilution refrigerators soon followed. As they became easier and more reliable to use, they supplanted the ^{3}He refrigerator. For polarizing, temperatures in the range of 200–400 mK could be maintained and lowered to ≈50 mK for frozen-spin operation when the microwaves were turned off. This added flexibility and ease of operation, similar to a ^{3}He refrigerator, has made the dilution refrigerator the current choice for a large range of polarized target experiments.

In the late 1970s, it also became clear that further improvements for polarized target experiments could only by achieved through new target materials with an increased polarizeable nucleon content. Today target materials such as NH_3, ND_3 and ^{6}LiD are available, which are radiation doped for the DNP process. Due to its very high polarization resistance against radiation damage, ammonia is the standard target material for the latest deep inelastic polarized

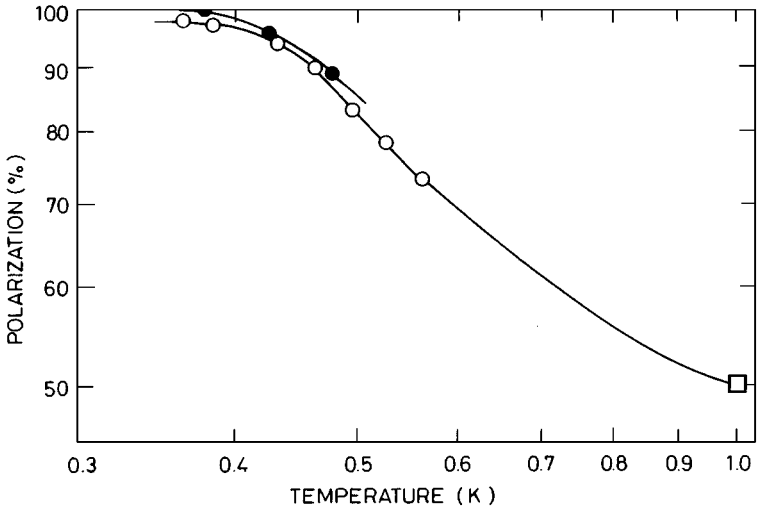

Figure 6 Positive ○ and negative ● polarizations observed in propanediol as a function of lattice temperature T_L.

electron-nucleon experiments (see Section 5), whereas ^{6}LiD has just started to be used in future experiments[1] of this type (24). In the present-day materials, a proton polarization of nearly 100% and a deuteron polarization of more than 50% have been obtained using superconducting magnets with magnetic fields ranging from 2.5 to 5 T or even higher.

Finally, another polarization scheme should be mentioned. This is the spin refrigerator concept (25), in which the electron polarization is transferred to the nucleons without microwaves and with no constraint on magnet uniformity. The technique relies on rotating a crystal of yttrium ethyl sulfate [$(C_2H_5SO_4)_3 \cdot 9H_2O$], doped with ytterbium (Yb), at liquid helium temperatures in a magnetic field. At a rotation of $\sim$90 Hz, the electron polarization of the Yb is approximately constant, and the Yb ion can transfer this polarization through dipole-dipole coupling to a nearby proton. Proton polarizations of 60–80% (26) and in excess of 50% (27) have been reported in two different systems. After the proton has been polarized, the magnetic field is reduced and the polarization held because of the long relaxation time. One disadvantage is that in order to reverse the polarization, the magnetic field must also be reversed. Such targets can be used as a cheaper alternative to dilution refrigerator-based frozen-spin targets where large acceptance is required.

[1]Experiment E155 at SLAC used ^{6}LiD and ammonia.

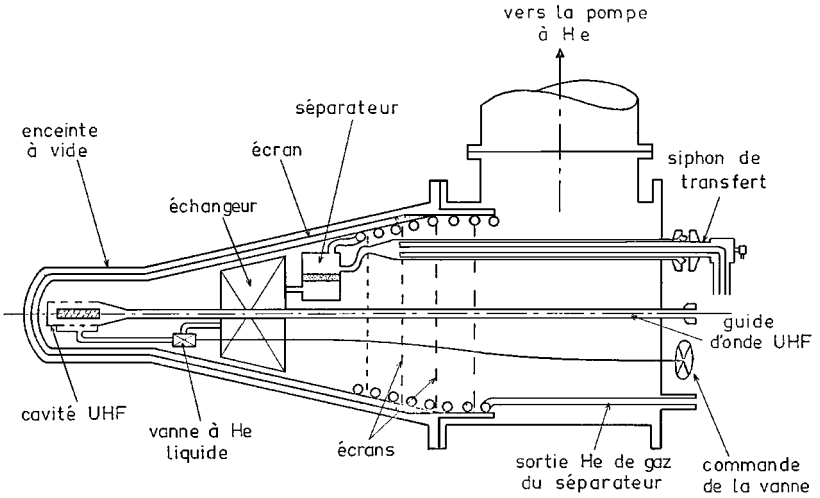

Figure 7 Schematic of the ^{4}He refrigerator described in [Ref. 28]. siphon de transfert = transfer siphon; vers la pompe à He = to the He pump; separateur = separator; écran = shield; exchangeur = exchanger; enceinte à vide = vacuum enclosure; vanne à He liquide = liquid helium (needle) valve; sortie He de gaz du separateur = exit for the separator helium gas; commande de la vanne = valve control; cavité UHF = UHF microwave cavity; guide d'onde UHF = UHF microwave guide.

3.1 *Cryogenics*

^{4}He AND ^{3}He EVAPORATION REFRIGERATORS This type of refrigerator, designed by Roubeau (28) and shown in Figure 7, was used in the first polarized target experiment (1).

Here, liquid ^{4}He is fed into a separator pot where the liquid phase is separated from the vapor phase by a sintered copper plate. The cold vapor is pumped away and used to cool the radiation shields and baffles that intercept the radiation heat load. Liquid helium flows through the separator plate into a heat exchanger and then is metered into the target holder (or evaporator) via a needle valve. The pool of liquid in the target holder is pumped on by large capacity Roots pumps to reduce the temperature to $\leq$1 K. As the cold vapor is pumped away, it exchanges heat with and cools the incoming warm liquid. Services such as microwaves and NMR are also brought into the target cavity. Because of the thermal properties of liquid helium, cooling powers of $\approx$2 W can be achieved with sufficiently large pumps and can withstand high heat input from particle beams. For the best polarization performance, it is necessary to operate the refrigerator with a high magnetic field, as is the case with the University of Virginia target operating at SLAC. This is discussed in Section 5.

In the ^{3}He evaporation refrigerator, a ^{4}He refrigerator as described above is wrapped around and mechanically isolated from the ^{3}He section. In a more elegant version by Herr & Kadansky (29), the ^{4}He-part is directly incorporated into the ^{3}He-refrigerator. The incoming ^{3}He gas is cooled and eventually liquified by the ^{4}He section, and it proceeds via heat exchangers and a metering valve into the target holder in a similar way to that described for the ^{4}He refrigerator. The liquid ^{3}He is pumped on by sealed Roots pumps to obtain temperatures of $\approx$0.5K. Because the gas is costly, it is recirculated through the refrigerator in a sealed system, which includes the pumps. ^{3}He refrigerators are now rarely used in polarized targets because of the versatility of dilution refrigerators.

^{3}He/^{4}He DILUTION REFRIGERATOR The operation of a ^{3}He/^{4}He dilution refrigerator is based on special properties of liquid mixtures of ^{4}He and ^{3}He. Above 0.88 K ^{4}He and ^{3}He are mixable in any ratio, whereas below 0.88 K the liquid consists of two separate phases: a diluted phase, which is ^{3}He poor, and a ^{3}He-rich concentrated phase (30). Important for the operation is the fact that in the diluted phase there is a reasonable amount of ^{3}He (6.4%), down to the lowest temperatures, that can be pumped and used for cooling. The cooling takes place when a ^{3}He atom is removed from the concentrated phase to the diluted phase. The dilution unit of a ^{3}He/^{4}He refrigerator consists of a mixing chamber, containing the target material, a heat exchanger and a still. The still temperature is normally adjusted via a heater to 0.8 K. Because of its much higher vapor pressure, compared to ^{4}He, the ^{3}He is preferentially boiled off and recirculated. It is liquified inside the refrigerator by heat contact with a separate ^{4}He circuit and then proceeds through different heat exchangers into the mixing chamber where the target material can be cooled to about 50 mK. A remarkable cooling power can be attained even at the lowest temperature by the development of special heat exchangers for the dilution part (31, 32). The cooling power of the world's largest ^{3}He/^{4}He dilution refrigerator is about 1 mW at 50 mK, 15 mW at 100 mK, 400 mW at 300 mK, and reaches 1.3 W at 500 mK; a set of eight Roots pumps in series with a nominal pumping speed of 13,500 m^3/h for ^{3}He is used (33). Nowadays target volumes between 0.2 cm^3 and 3000 cm^3 can be handled by fast loading the mixing chambers of various types of ^{3}He/^{4}He dilution refrigerators (31, 34). These are the standard devices for future modern experiments with low-intensity particle beams (see Section 5).

3.2 *Polarizing Magnets*

The polarization that can be obtained with a given material is linked to the value of B/T_L as is seen in Figure 6, which also emphasizes the fact that the spin temperature T_{SS} (hence polarization) depends on the lattice temperature T_L. Early polarized targets used iron magnets operating at fields of 2–2.5T and

operated at temperatures of 1–1.5K so that $\frac{B}{T_L}$ was ≈2. The development of low-temperature refrigerators and high-field superconducting magnets meant that $\frac{B}{T_L}$ of 50 - 100 were easily achievable. But for various technical reasons DNP works best when $\frac{B}{T_L} \approx 5$–10.

The main limitation of iron magnets is that, in order to boost the operational field to 2.5 T and maintain the required uniformity, a substantial mass of iron and copper coil restricts access and reduces the acceptance of the experiment. This is particularly true if the polarization direction is required to be in the plane of scattering. Superconducting magnets that could be built with large material-free apertures changed this. Magnets built in the Helmholtz configuration that have a 100° aperture for scattered particles in the forward direction and about 35° for scattering near 90° are now available (35).[2] Nearly a 4π aperture for the outgoing particles can be achieved by operating the targets in the frozen-spin mode (see Section 4). For such applications superconducting solenoid magnets are available up to 7 T, [3] which must be used in particle experiments together with so-called holding magnets (see Section 5).

3.3 *Microwaves*

The frequency needed for DNP is about 28 GHz/T, i.e. 140 GHz at 5 T. The required power at a temperature of 1 K is 1–2 mW/g of target material at 2.5 T (70 GHz) and ≈ 20 mW/g at 5 T (140 GHz). The highest power devices available at these frequencies are extended interaction oscillators (EIO);[4] for lower power applications, klystrons, IMPATT, and Gunn diodes are available. Carcinotrons, which used to be the tubes of choice, are no longer manufactured. The power that can be extracted from a tube is inversely related to its operational frequency, and the power absorption in microwave components increases with frequency. Therefore, from the standpoint of microwave power, there is a practical limit for operation at about 210 GHz, corresponding to 7.5 T, unless very low-mass targets are being considered.

The power supply for a given tube should be capable of frequency modulating the microwaves by up to about ±40 MHz around the central frequency. Substantial improvements in maximum polarizations and increased polarization rate have been observed with the frequency modulation method (36).

3.4 *Nuclear Magnetic Resonance and Polarization Measurement*

A spin-I system placed in a magnetic field $\vec{B}$ shows a Zeeman energy splitting into $2I + 1$ levels. These levels are separated in energy by $\hbar\omega_L = \vec{\mu}\vec{B}/I = g\mu_n B$ where g is the g-factor of the particle with spin I and μ_n is the nuclear

[2]Oxford Instruments, Eynsham, Oxon, UK.
[3]STCM STIPE at CEN Saclay.
[4]CPI (Canada), Georgetown, Ontario, Canada.

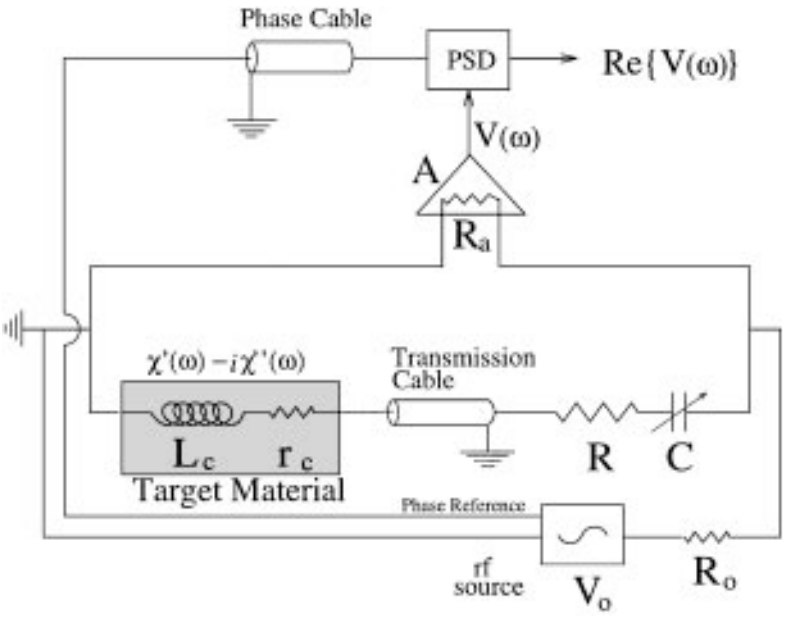

Figure 8 Schematic drawing of the Q-meter (NMR) circuit.

magneton. When the spin system is irradiated by an rf field at the Larmor frequency, the spin system either absorbs some energy or the rf induces the spin system to emit energy. The response of a spin system to rf irradiation is described by its magnetic susceptibility $\chi(\omega) = \chi'(\omega) - i\chi''(\omega)$, where $\chi'(\omega)$ is the dispersive and $\chi''(\omega)$ the absorptive part of the susceptibility. The absolute polarization of the material is proportional to the integral of the absorptive part of the susceptibility (37).

$$P = K \int_0^\infty \chi''(\omega)\, d\omega. \qquad 4.$$

K is a constant containing the properties of the NMR system concerned.

The polarization is measured by the nuclear magnetic resonance (NMR) method, using a series Q-meter (38), as shown in Figure 8. Here, the Q-meter is connected to an NMR-coil with inductance L_C and resistance r_C, that surrounds or is embedded in the target material via a coaxial transmission cable, capacitor C, and damping resistance R that forms a series LRC circuit. Through the inductive coupling between the spins and the coil, the impedance of the coil will become (15)

$$Z_C = r_C + i\omega L_C(1 + 4\pi\eta\chi(\omega)), \qquad 5.$$

where η is the filling factor of the coil. As shown in Figure 8, the circuit is driven by a frequency synthesizer V_0, which sweeps the rf frequency ω through the Larmor resonance. This causes a change of the inductance of the coil as the target material absorbs or emits energy. The inductance change in turn causes an impedance change in the circuit, which is proportional to the complex output voltage $V(\omega, \chi)$ as long as the current is kept constant. At the last stage, a phase-sensitive detector (PSD) allows the selection of the real part of the voltage by using the input rf signal as a reference. The voltage is a superposition of both the signal, proportional to χ, and the so called Q-curve, which is the response of the Q-meter to ω in the absence of χ. The Q-curve is measured by setting the B-field so that the Larmor frequency ω_L of the spin species is well outside the range of the frequency scan of the Q-meter, where χ'' vanishes and χ' is negligible. The two signals are subtracted and the result is the NMR-signal,

$$S(\omega) = Re\{V(\omega, \chi) - V(\omega, 0)\} \approx \chi''(\omega). \qquad 6.$$

The polarization is calibrated using the calculable polarization P_{TE} (Equation 2) at thermal equilibrium (TE) of the nuclear spins and at the known lattice temperature in a known magnetic field. This is normally done at temperatures in the range 1–2K, where the polarization build-up time is short (less than a few hours). The absolute polarization P is finally obtained by comparing the TE-signal area $\int S_{TE}(\omega)d\omega$ with that of the enhanced signal area $\int S_{enh}(\omega)d\omega$ under microwave irradiation,

$$P = \frac{\int_0^\infty S_{enh}(\omega)\, d\omega}{\int_0^\infty S_{TE}(\omega)\, d\omega} P_{TE} \qquad 7.$$

The polarization can be monitored continuously or sampled. Typical highly polarized NMR signals of protons and deuterons are shown in Figure 9.

The polarization accuracy $\Delta P/P$ is about $\pm 2\%$ for protons and ± 2–4% for deuterons. This is achieved by a precise measurement of the temperature and a careful tuning of the NMR-circuit to avoid gain ratio errors of the low frequency amplifiers and non-linearities of the high frequency amplifiers. In addition, the TE signal errors are reduced by using the signal averaging technique to overcome the signal-to-noise ratio problem, which is extremely serious in the case of the deuteron polarization determination. Details about NMR techniques can be found in References (39–45).

Finally it should be mentioned that the measured polarization $P_Z(D)$ of the deuteron is not identical with that of the neutron P_Z(N). The quantum mechanical calculation using Clebsch-Gordan coefficients shows that 75% of the neutron spins in the D-state are antiparallel to the deuteron spins (46). So

$$P_z(N) = (1 - 1.5\,\alpha_D) P_z(D) \approx 0.91 P_Z(D), \qquad 8.$$

where α_D is the probability of the deuteron to be in a D-state.

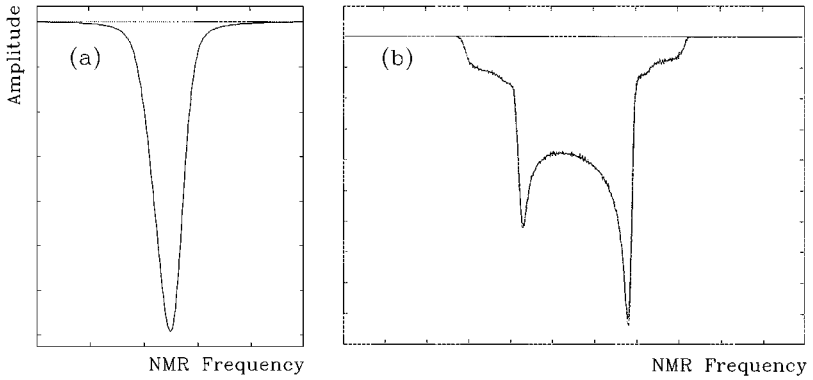

Figure 9 Dynamically enhanced NMR signals of proton (*a*) and of deuterons (*b*), which see a nonvanishing electrical field gradient at their sites. Polarization correspond to 92% for protons and 37% for deuterons.

3.5 *Target Materials*

Important criteria for the choice of a material suitable for nuclear particle physics experiments are (*a*) the degree of polarization P, and (*b*) the dilution factor f, which is the ratio of free polarizable nucleons to the total number of nucleons.

When a polarized target (e.g. a proton target) is used in a scattering experiment, a scattering asymmetry A (47) is measured when the number of events $N\uparrow$ scattered in one direction is compared with the number $N\downarrow$ scattered when the spin is reversed. For a pure, 100% polarized target, the physics asymmetry A is given by $A = \frac{\sigma\uparrow - \sigma\downarrow}{\sigma\uparrow + \sigma\downarrow}$.

With practical polarized targets, however, a counting rate asymmetry $\epsilon = \frac{N\uparrow - N\downarrow}{N\uparrow + N\downarrow}$ is measured and is related to A by

$$A = \frac{1}{Pf} \frac{N\uparrow - N\downarrow}{N\uparrow + N\downarrow}, \qquad 9.$$

where f and P correct for the fact that the target is not 100% pure nor 100% polarized. Since $N\uparrow + N\downarrow$ is proportional to the measuring time, the beamtime t to reach a certain statistical error ΔA shows the following dependency on material properties

$$t^{-1} \propto \rho(f \cdot P)^2, \qquad 10.$$

where ρ is the density of the material. This expression shows the importance of the values P and f, which have to be optimized.

Further important requirements for the use of a polarized target material are (*a*) simple target preparation and ease of handling; (*b*) short polarization build-up time; (*c*) good polarization resistance against radiation damage, with the possibility to repair the radiation damage (see Section 3.7); and (*d*) presence of other polarizable nuclei.

CHEMICALLY DOPED MATERIALS The very nature of the DNP process as described in Section 2 demands that a paramagnetic dopant be introduced into the host target material. A priori, it cannot be predicted which host and dopants are best matched. Even in the early days there was considerable study before it was determined that LMN doped with neodymium could produce proton polarizations of $\pm 70\%$. The materials used in current polarized targets were only established after many measurements of combinations of host and dopant (17, 48). For example, butanol is combined with porphyrexide, which is easily mixed in. On the other hand, the diols, including the deuterated forms, worked best with a chromium radical Cr(V) that was introduced via a chemical reaction. Then EHBA, a synthesized form of Cr(V), was introduced (49), followed later by its deuterated counterpart EDBA (50). This form was mixed in solution with the host, which allowed better control of the doping.

The solid target materials have to be in the form of small pieces, preferably of equal sizes, to provide good and uniform cooling of the material with the liquid helium. For example, 1-butanol containing 5 wt% of water and 4 wt% of EHBA-Cr(V) as the paramagnetic dopant is now an often used material. All the components are either normal or deuterated. Butanol is preferred because, compared to ammonia, it lacks a polarized background and, compared to propanediol, its dilution factor is higher. The material is frozen into spherical beads of about 1.5 mm in diameter by dripping the liquid mixture into liquid nitrogen. Rapid freezing ensures that the material transforms into a glassy state, which is required for the homogeneous distribution of the paramagnetic radicals. Details about the preparation method are given in (51, 52).

Some materials (53) must be handled at temperatures below that of liquid nitrogen to maintain their amorphous character, while others are spontaneously combustible (54) when exposed to air; neither characteristic lends itself to confidence in being able to produce an operational target.

On the other hand, pentanol-2 stays amorphous up to room temperatures and, when doped with EHBA, has produced polarizations of $\approx 85\%$ in a dilution refrigerator (55).

Recently, the first results of DNP have been obtained in thin polymer foils and tubes (56–58). Protons, deuterons, and ^{19}F have been polarized at 2.5 T and below 0.3 K using the stable nitroxyl radical TEMPO (59, 60). This

Table 1 Polarized target materials commonly used in particle scattering experiments

Materials and chemical composition	Dopant[a] and method	Polarizable nucleons % by weight	B/T Tesla/K	Polarization %	Radiation characteristic flux[b] 10^{14} particles/cm^2
LMN	Neodymium	3.1	2.0/1.5	± 70	$\sim$0.01
$La_2(Co, Mg)_3(NO)_3 \cdot 24H_2O$	Ch				
1,2 Propanediol	Cr(V)	10.8	2.5/0.37	$+98$	$\sim$1
$C_3H_6(OH)_2$	Ch			-100	
1,2 Ethanediol	Cr(V)	9.7	2.5/0.5	± 80	$\sim$2
$C_2H_4(OH)_2$	Ch				
Butanol	EHBA Cr(V)	13.5	2.5/0.3	± 93	3$-$4
C_4H_9OH	Ch				
EABA	EHBA Cr(V)	16.5	2.5/0.5	$+75$	7(+), 3.5($-$)[c]
$C_2NH_7BH_3NH_3$	Ch			-73	
Ammonia	$NH_2\bullet$	17.5, 16.6	5.0/1.0	$+97$	70, 175[d]
$^{14}NH_3$, $^{15}NH_3$	Ir			-100	
d-Butanol	EDBA	23.8	2.5/0.3	± 50	Not measured
C_4D_9OD	Ch				
d-Ammonia	$ND_2\bullet$	30.0, 28.6	3.5/0.3	$+49$	130(+), 260($-$)
$^{14}ND_3$, $^{15}ND_3$	Ir			-53	
Lithium deuteride	f-center	50	6.5/0.2	± 70	400
^{6}LiD	Ir				

[a]Ch: chemically doped, Ir: doped through irradiation.
[b]The radiation dose which reduces the polarization by e^{-1} of its value.
[c]For positive and negative polarizations, respectively.
[d]In NH_3 there are two distinct regions of decay.

radical can be easily introduced via a diffusion process. In addition, some promising first results were obtained by doping an organic scintillator material with TEMPO. Mango and co-workers (S. Mango, personal communication) at PSI were able to extract scintillator light from a 10 x 10 x 1 mm^3 sample that had been polarized to 55% at 0.3 K and 2.5 T. Such polarizable materials, which are solid and can be handled at room temperature for at least several hours, could provide new experimental possibilities in nuclear and particle physics along with their obvious practical advantages in the loading of refrigerators.

Table 1 lists the properties of the most common target materials used in polarization experiments, and Figure 10 shows a typical polarization build-up curve for butanol and its deuterated complement (20).

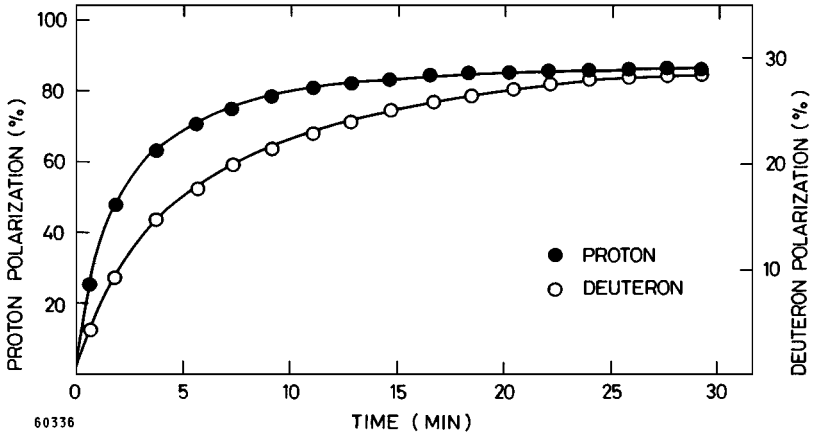

Figure 10 Polarization build-up of the proton and deuteron in butanol and deuterated butanol, respectively.

RADIATION-DOPED AMMONIA TARGETS Another method to introduce the paramagnetic radicals into solidified target materials (frozen beads or chips) is to irradiate the pure samples. This preparation technique for the DNP was first successfully used with NH_3 (61) and ND_3 (62, 63). Two different irradiation techniques can be employed, and both make use of high-intensity ionizing particle beams to produce an adequate number of radicals (some 10^{19} spins/ml) in a reasonable amount of time: (*a*) high-temperature irradiation at 80 - 90 K; and (*b*) low-temperature irradiation at 1 K.

Low-temperature irradiation means that the radicals necessary for DNP are produced during the experiment. As high radical densities are wanted in order to reduce polarization build-up time, this preparation method is only suitable in combination with high-intensity beams of ionizing particles, such as electrons or protons.

Detailed studies have shown that it is more advantageous to operate with high-temperature pre-irradiated material (64, 65). The accumulated flux on ammonia, obtained with high-intensity electron beams from injection linacs, e.g. the 20 MeV injection linac of the BONN electron accelerator or the 30MeV SUNSHINE facility at Stanford University, is $10^{16} - 10^{17}$ electrons/cm^2. Detailed information about the ammonia preparation for DNP can be found in the work of Brown et al (66). Electron spin resonance (ESR) measurements performed with high-temperature irradiated NH_3 and ND_3 have indicated that the radicals NH_2 and ND_2, respectively, are responsible for DNP in ammonia (67, 68). If the samples are kept under liquid nitrogen, the lifetimes of the radicals are in the order of years.

As experience shows, ND_3 target preparation is more difficult compared to that of NH_3. The temperature at which the radicals are produced is decisive. High deuteron polarization values ($\geq$30%) in high-temperature irridiated material can only be achieved by means of an additional low-temperature irradiation (68, 69, 35). In the case of electron beams, the typical beam flux to achieve best deuteron polarization values is about $4 \cdot 10^{14}$ e^-/cm^2 (69), to 10^{16} e^-/cm^2 (35).

A disadvantage of ammonia compared to alcohol and diol targets is the existence of polarized background nuclei ^{14}N (spin-1) or ^{15}N (spin-1/2) in $^{14}NH_3$, $^{15}NH_3$, $^{14}ND_3$, and $^{15}ND_3$. ^{15}N polarization is relatively easy to measure (35) but the ^{14}N nucleus, whose quadrupole moment is about 10 times larger than that of the deuteron, challenges the NMR measurement. With a combination of techniques, this problem was solved (21).

RADIATION-DOPED LITHIUM HYDRIDES AND DEUTERIDES Pioneering work to prepare ^7LiH, ^6LiH, and ^6LiD for the DNP process has been done by different groups at Saclay (70–73) and recently in Bonn (74). At room temperature, the lithium compounds are in their solid state phase, and the paramagnetic impurities (so-called F-centers) are introduced by irradiation. In contrast to the ammonia targets, the temperature before irradiation has to be 180 ± 2 K where the F-center production efficiency and the targets' mobility and agglomeration probability during the irradiation become optimum for the DNP process.

^6LiD is of special interest as a polarized neutron target with its high dilution factor $f = 0.5$ for neutrons. Here it is assumed that ^6Li is an alpha nucleus plus a deuteron. This simplified picture is supported by the fact that the magnetic moments of ^6Li and the deuteron differ only by about 3%. Theoretical studies by Schellingerhout et al (75) also support this view. A further advantage is the easy detection of the deuteron or ^6Li TE polarization signal; in LiD, there is no asymmetric splitting of the energy levels in these spin-1 systems due to the vanishing electrical field gradient in the face-centered, cubic lattice structure. Recent measurements demonstrate a high polarization resistance against radiation damage (74, 76).

3.6 *Polarization Build-Up Time*

It follows from the definition of the asymmetry that a change of the target polarization direction is necessary, and, to reduce false asymmetries to a very low level, this has to be done as often as possible. A fast polarization build-up time τ combined with a high polarization depends strongly on the paramagnetic radical density. The optimal density varies for different materials and is in the range of 10^{19}–10^{20} spins/ml. Finally, the magnetic field and temperature are crucial, e.g. τ is minutes at 1 K and 2.5 T but increases to hours when the temperature is reduced to 250 mK.

3.7 *Radiation Damage*

Polarization is reduced by radiation damage and is a serious problem in experiments performed with the alcohol and diol materials where the radicals for the DNP process are provided by chemical dopants. This phenomenon can be understood qualitatively as follows.

Additional radicals in the target materials are created during the irradiation. These radiation-produced radicals normally have a different g-factor. Compared to the Larmor frequency of chemically induced radicals, the frequency of radiation-produced ones is changed and these additional radicals do not contribute to the DNP process. As radical density increases, it affects the relaxation processes so that the nucleon relaxation time is shortened and nucleon polarization is reduced.

In most cases, however, this polarization reduction can be almost recovered by heating or annealing the target material up to, but not higher than, the devitrification temperature (48). Part of the polarization is not recovered at each anneal, and the target material has to be changed after about six anneals. The polarization decrease combined with the time-consuming annealing process limited the use of these alcohol and diol materials in experiments with intense proton, electron, or photon beams.

At this point the development of ammonia, with its high polarization resistance to radiation damage, made it the choice for improved experiments of a new generation (see Section 5). It turned out that the depolarizing dose in NH_3 is more than an order of magnitude higher compared with that of butanol (64, 65). In addition, the polarization loss in NH_3 can be completely recovered by annealing the sample at a lower temperature ($\approx$77K) than in the case of a butanol sample ($\approx$120 K) and can be repeated many times without loss. The initial increase of deuteron polarization during an experiment is completely different from that observed for the alcohol materials and NH_3. The hypothesis of a change in the dominant DNP process in ND_3 during the further irradiation (where additional and new deuterated radicals are created) is supported by a remarkable shift of the optimal microwave frequency (64). Taking all results together, it is clear that the high polarization resistance to radiation damage in ammonia is mainly a consequence of the initial radiation doping of radicals.

4. FROZEN SPIN TARGETS

4.1 *Dynamically Polarized*

The development of ^{3}He/^{4}He dilution refrigerators (32) with a base temperature of 50 mK or lower allowed an additional operation mode of polarized targets and made new types of experiments possible. Polarized targets with ^{4}He or ^{3}He

evaporative cooling have to work in a continuous mode, i.e. with permanent microwave irradiation to maintain the DNP process at 1 K or 0.5 K, respectively. At these temperatures the nucleon polarization relaxation time T_1 is relatively short. This continuous mode operation puts strong constraints on the design of polarizing magnets. Due to the field homogeneity requirements over the entire target volume, the large dimensions of the magnet coils limit the angles for the outgoing particles. This is a serious problem for experiments performed with low-intensity beam, e.g. ace-tagged photon beams. To obtain a reasonable counting rate, a wide opening angle with the ability to simultaneously measure a large kinematical range is needed. This can be achieved through the concept of the frozen spin target.

The operation of the frozen spin target is based on the experimental fact that the nucleon polarization relaxation time T_1 is a very strong function of the temperature and magnetic field. T_1 characterizes the polarization decay after switching off the DNP mechanism (microwaves). Typical values for T_1 are minutes at a temperature of 1 K and days below 100 mK. The principle of the frozen spin target operation is to polarize the target material at a high field (e.g. 5 T) and in the temperature range 0.3–0.5 K. Once the target material is optimally polarized, the microwaves are switched off, and the polarization is frozen at temperatures around 50 mK (frozen spin mode). Due to the long proton T_1 at these temperatures, it is possible to reduce the field to a value where the polarization is acceptable (holding field).

An appropriate setting of the holding magnets allows the target polarization to be oriented in different directions (77, 78) and provides good experimental access (see Figure 11).

With a target temperature around 50 mK, the holding field can be 0.3-0.4 T with an acceptable decay of the polarization. Since the cooling power of the ^{3}He/^{4}He dilution refrigerators operating at such temperatures is relatively low and the Kapitza resistance (30) large, the beam intensity for experiments with a frozen spin target is limited. The maximum flux hitting a target area of 1 cm^2 is 10^7–10^8 particles/sec (77, 79).

At present, frozen spin targets for experiments are installed in Bonn (80), Dubna (81), PSI (78), Saclay (77), TRIUMF (82), and KEK (83). A new concept of a small superconducting holding magnet placed inside a polarizing refrigerator has been developed (82, 84) and was successfully used in first particle experiments at Bonn (10) and on LEAR (CERN). The coils can be wound as a solenoid or in a split-pair configuration on the inner radiation shield of the refrigerator and can replace the external large superconducting holding magnets (see Figure 12). The fringe field and its influence on nearby detector components is minimized and that makes it possible to operate polarized solid targets in a 4π-detector (see Section 5).

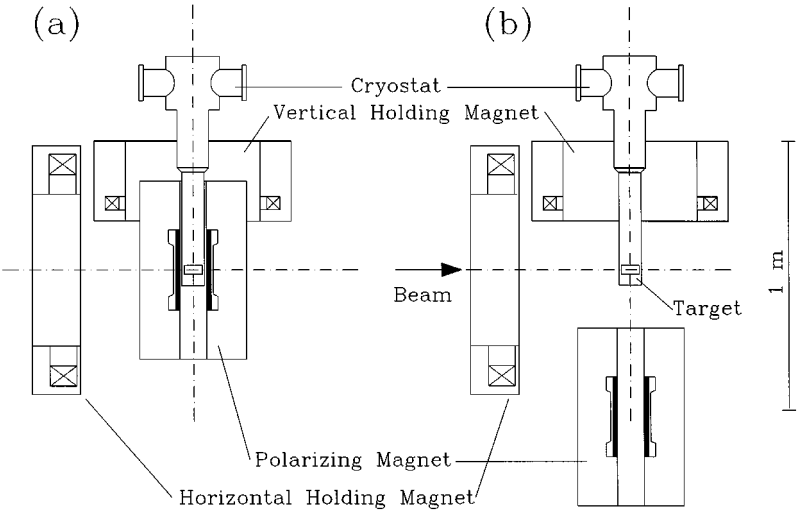

Figure 11 Set-up of a frozen spin target in the 'polarization mode' (*a*) and in the 'holding mode' (*b*), in which a vertical as well as a horizontal spin direction can be realized.

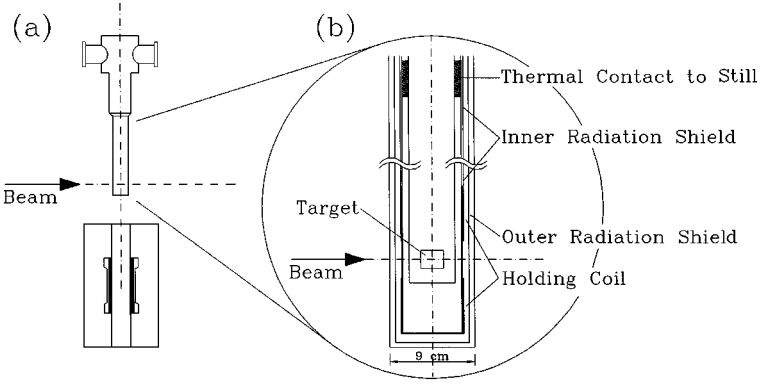

Figure 12 'Holding mode' (*a*) of a frozen spin target with an internal superconducting 'holding coil'; (*b*) shows a close-up of the target area. This concept was used for the measurement of the eta photoproduction on polarized protons at the Bonn tagged photon facility (see Section 5.1).

Finally, it should be mentioned that for an optimal operation of a frozen spin target the so-called superradiance effect (85, 86) has to be considered. This polarization-destroying effect occurs only at negative polarization and can be avoided by a proper tuning of the NMR system (87) or magnetic field manipulations (41).

4.2 *Brute Force Polarized*

The method of brute force (or equilibrium) polarization works for every polarized target material. From Equation 2, it follows that, to get high polarizations, very high magnetic fields and very low temperatures are required. In addition, as mentioned earlier in Section 2, molecular hydrogen cannot be used because of the ortho to para conversion at low temperatures. However, in 1967 Honig (88) proposed polarizing frozen HD by the brute force method. An HD target is attractive because (*a*) the molecule is polarizable at low temperatures; (*b*) it has a high dilution factor; (*c*) it contains one neutron, and that can be polarized; and (*d*) as it has turned out, the degree of polarization of both the H and D can be manipulated independently. The drawback of the brute force method is that it takes HD a very long time to reach thermal equilibrium at the value of B/T_L necessary for high polarizations because the molecule is very weakly coupled to the lattice. However, doping with small concentrations ($\approx 10^{-4}$) of ortho-H_2 or para-D_2 (88) to allow spin lattice coupling has led to a faster polarization build-up. This is similar to the situation in DNP targets where the doping leads to faster relaxation to TE. For the HD case, as the polarization builds up, the doped impurities decay to magnetically inert states, the relaxation time T_1 becomes very long again, and the spins are frozen.

The proton polarizations obtained this way are high, ≈80%, but the deuteron polarizations are only about 20%. Moreover, these polarizations are achieved only after waiting for several decay constants of the impurities. For o-H_2, with a constant of 6.25 days, holding at high field and low temperature (typically 17 T and 15 mK) for 3 to 4 weeks is practical, but for p-D_2, with a constant of 18.2 days, holding for months is not.

The solution (89) is to use o-H_2 to build up the proton polarization and then, by a technique of adiabatic fast passage, transfer the polarization to the deuteron. This method takes advantage of the dipolar coupling of H and D nuclei in different HD molecules. The process can be repeated several times and deuteron polarizations of about 50% can be expected. The target is maintained at 17 T and 15m K for 40–50 days until the T_{1D} becomes extremely long again. After this, the target is extracted from the production cryostat, using a special retrieval cryostat, and stored and/or transported in a holding dewar. Finally, the target material can be installed in the in-beam refrigerator and magnet for experiments. The holding temperature and field will depend on the experimental

configuration, but 0.5 K and 1–2 T will allow a sufficiently long lifetime to perform most experiments. The target itself is not completely pure HD since there are about 5–10% of aluminum wires imbedded to remove the heat of conversion of o-H_2 to p-H_2. Secondly, it is obvious that additional heat input into the target will accelerate the polarization decay so such a target can only be used in a low-intensity photon beam or neutron beam. If for any reason the polarization dies, there is no way of replenishing it, and it must be changed, unlike the case of DNP frozen spin targets. Using this operational procedure, four targets can be made at the same time so that they can be stockpiled for an experiment. Within the next year the SPHICE collaboration (90) will use such a target in a measurement of the Gerasimov-Drell-Hearn (GDH) sum rule at the LEGS facility at BNL, and a measurement is proposed at GRAAL (Grenoble) (91).

5. POLARIZED TARGET EXPERIMENTS

As already mentioned in the Introduction, spin effects using polarized solid targets have been studied in innumerable experiments. The latest results obtained at laboratories that have operated polarized proton and deuteron targets over the last 10 years, i.e. Bonn, Brookhaven, CERN, Dubna, Gatchina, KEK, Kharkov, LAMPF, IHEP Serpukhov, PSI, Saclay, SLAC, and TRIUMF, are given in the proceedings of several symposia (92–96). During the last several years, upgraded and improved accelerators, e.g. cw-electron machines, have been built and have started operation. Electron beam polarization technology has also made rapid progress with optical pumping of strained GaAs photocathodes, which yields 80% polarization. (Double) polarization experiments are now planned or under way that address fundamental questions in nucleon and nuclear structure and use real and virtual photons as probes. Table 2 lists

Table 2 Experimental sites with polarized solid state targets performing experiments with electromagnetic probes

Laboratories	Physics goals
CERN (Geneva)[a]	Nucleon spin structure
ELSA (Bonn)[a]	Nucleon resonances, GDH
GRAAL (Grenoble)	GDH
TJNAF (Newport News)	Nucleon resonances, GDH, formfactors, nucleon spin structure
LEGS (Brookhaven)	GDH
MAMI (Mainz)	Nucleon resonances, GDH, formfactors
SLAC (Stanford)[a]	Nucleon spin structure
SPRING8 (Osaka)	GDH

[a]Currently running polarized targets.

the various experimental sites where experiments with polarized targets using electromagnetic probes will be performed.

In the following we discuss some modern polarized solid target equipment, which is used to address some physics goals at various laboratories.

5.1 *Photoproduction at the Bonn Tagged Photon Facility*

Experimentally, photo and electronuclear reactions are a particularly clean instrument to investigate the resonance region and to analyze the multipole content of the individual resonance contributions. With the advent of the new electron facilities, each with large duty-factors, new classes of experiments, including polarization degrees of freedom, have become possible. Such investigations range from threshold production of mesons to detailed studies of the helicity structure in the resonance region.

Pilot experiments with polarized targets have been performed at the Bonn electron accelerator ELSA. Target asymmetry data for the reactions $\gamma p \uparrow \rightarrow \pi^+ n$ and $\gamma p \uparrow \rightarrow \pi^0 p$ were taken simultaneously with the PHOENICS detector using tagged photons up to 950 MeV. The large angular acceptance of the detector could be retained with the polarized target by employing the technique of the frozen spin target (see Section 5). The set-up of the frozen spin target is shown in Figure 11. Special efforts were made to minimize the various wall thicknesses around the polarized target material to reduce unwanted background reactions. Details about the special target area design are given in Reference (97). The target itself was a 4 cm long, 2.5 cm diameter cylinder filled with beads of butanol. It was polarized in a magnetic field of 5 T. During the data-taking period, the spin orientation has been maintained by means of the vertical holding magnet at a field of 0.35 T. At a temperature of about 60 mK, the proton polarization relaxation time T_1 was longer than 5 days. An average polarization of $P = 85\%$ and a maximum polarization of $P = 98\%$ were achieved. Detailed information and the results of the experiment are given in the work of Dutz et al (79). The position and the geometry of the large external superconducting holding magnets together with its fringe field did not allow the placement of detector components close to the target region. This was required for the target asymmetry measurement of the reaction $\gamma p \uparrow \rightarrow \eta p$, especially for the detection of the $\eta \rightarrow \gamma\gamma$ decay. A top view of the experimental set-up at ELSA is shown in Figure 13.

This first polarized target experiment belongs to a series of new and improved measurements designed to study eta photoproduction over a large kinematical range with the TAPS detector at MAMI (Mainz) and the PHOENICS experiment at ELSA (98). Based on the first experience with the internal coil concept (84), a thin superconducting coil has been wound in a split-pair configuration on the inner cooling shield of the dilution refrigerator. The cooling of the 100-μm

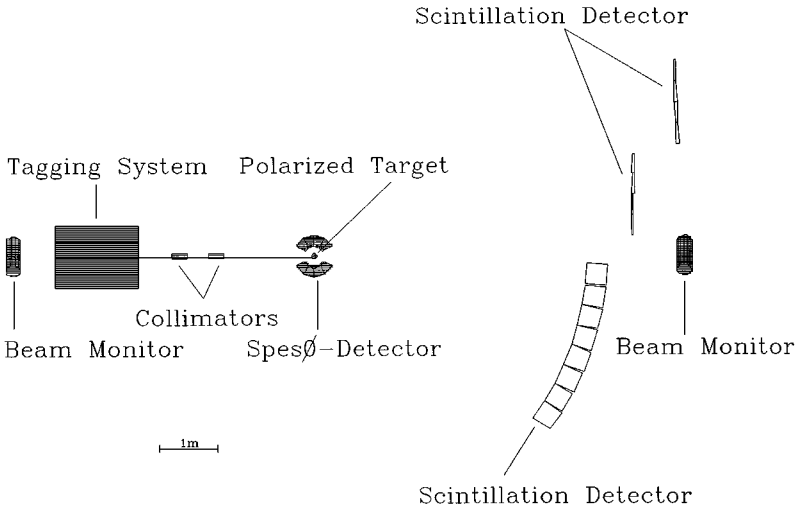

Figure 13 Detector and target set-up of the asymmetry experiments in the eta photoproduction on polarized protons at the Bonn PHOENICS experimental area.

thick NiTi wire to about 1.2 K has been provided by the contact of the copper carrier to the still. This internal magnet replaced the outer large vertical holding magnet used in the pion production experiments mentioned above. At a holding field of 0.4 T and a temperature of about 60 mK, the relaxation time for the proton polariaztion was approximately a week. The history of the polarization during a run period of two weeks is shown in Figure 14.

Asymmetry data from threshold to 1150 MeV have been taken at a tagged photon beam intensity of up to $5 \cdot 10^7$ photons/sec. The results of the experiment by Bock et al are given in (99).

Summarizing the operation of the polarized target experiments at the Bonn tagged photon beam facility, which compensates the low beam intensities ($<10^8$ photons/sec) by a simultaneous measurement over a large energy and angle range:

1. Solid polarized targets must be used that achieve a luminosity of higher than 10^{31}/(sec cm^2). Acceptable beam intensities are about $5 \cdot 10^7$ photons/sec hitting 1 cm^2 target area.

2. In exclusive reactions, kinematical overdetermination allows a clear event separation from background nuclei, which results in a dilution factor of nearly one.

3. Frozen spin target operation fulfills the requirement of a large angle detection.

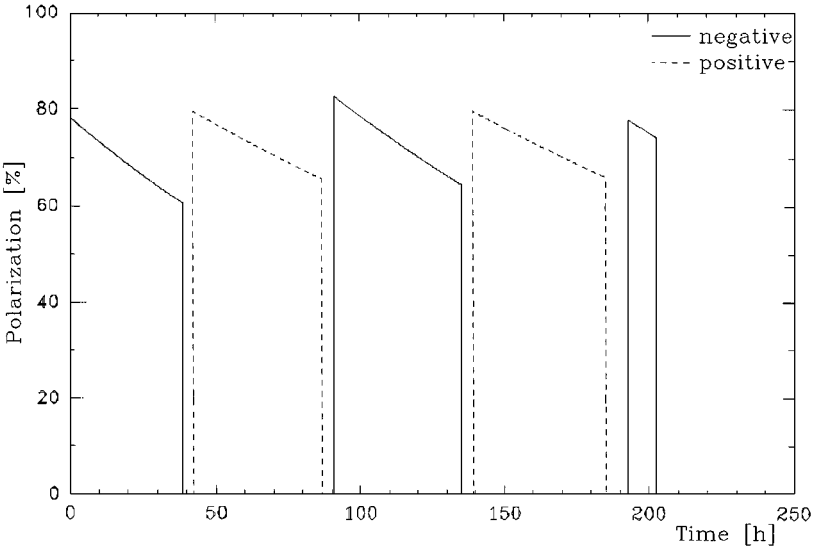

Figure 14 Polarization history for protons in the frozen spin mode at a 'holding field' of 0.4 T provided by an internal 'holding coil'. The data have been taken during the eta photoproduction experiment at ELSA (Bonn). The direction of the polarization has been changed every two days.

4. Frozen spin targets with internal holding coil equipment can be operated in 4π-detectors.

5.2 *Measurement of the Gerasimov-Drell-Hearn Sum Rule*

The Gerasimov-Drell-Hearn (GDH) sum rule relates the helicity asymmetry of the total cross section for polarized photons on polarized nucleons to the anomalous magnetic moment of the nucleon (100, 101). Being based on general principles of physics, the GDH sum rule is an important consistency check for the understanding of the hadronic structure. The GDH prediction was formulated in the 1960s, but has never been directly measured. However, an analysis of pion photoproduction by Karliner indicates some problems with the proton-neutron difference for the GDH sum rule (102). With the modern techniques to produce polarized beams and targets at the new electron accelerators, this situation is expected to change soon. There is a TJNAF proposal (103) to measure the helicity structure of pion photoproduction up to 2.3 GeV, and a collaboration at MAMI (104) plans to obtain new data from threshold to intermediate energies in addition to the direct measurement of the GDH sum rule. Of particular interest is the question whether the sum rule converges as a function of the excitation energy, and if so, how fast.

Additional interest in the GDH sum rule arose when Anselmino et al (105) formulated a connection with the polarized structure function g_1 of the nucleon in the attempt to understand the proton spin problem arising from the results of the EMC experiment (106). New results have been obtained from SMC and SLAC (see below) and HERMES (107) experiments at high Q^2. However, there also is a strong call for spin structure studies at low Q^2. An experiment has been proposed at TJNAF to study the region of $0.25\ \mathrm{GeV}^2 \leq Q^2 \leq 2\ \mathrm{GeV}^2$, which should show a rapid transition from coherent absorption to incoherent deep inelastic scattering reactions (108, 109). Latest results in this energy regime have been measured at SLAC (110). The GDH sum rule gives the prediction at $Q^2 = 0$ in the following way:

$$\int_0^\infty d\nu \frac{\sigma_{3/2} - \sigma_{1/2}}{\nu} = \frac{2\pi^2\alpha}{m^2}\kappa^2, \qquad 11.$$

where $\sigma_{3/2}, \sigma_{1/2}$ are the cross sections for parallel and antiparallel spin configurations of the photon and the nucleon, respectively. ν is the photon energy, m and κ are the mass and the anomalous magnetic moment of the nucleon. The proposed experimental test of the GDH sum rule thus requires the measurement of the helicity asymmetry of the total hadronic photoabsorption cross section over a wide range of photon energies, starting from the pion threshold. Measurements at MAMI (Mainz) in the domain of low photon energies (140–800 MeV) start in 1997 and will be continued at ELSA (Bonn) for higher energies up to 3 GeV. The detector set-up for the Mainz measurement is shown in Figure 15.

To reach the center of the DAPHNE detector, a special ≈2 m long ^{3}He/^{4}He refrigerator has been constructed, which incorporates the beam pipe in the backward region of the detector. The DAPHNE detector and a 6.5 T polarizing magnet (not shown in Figure 15) are mounted on a precise rail system and can

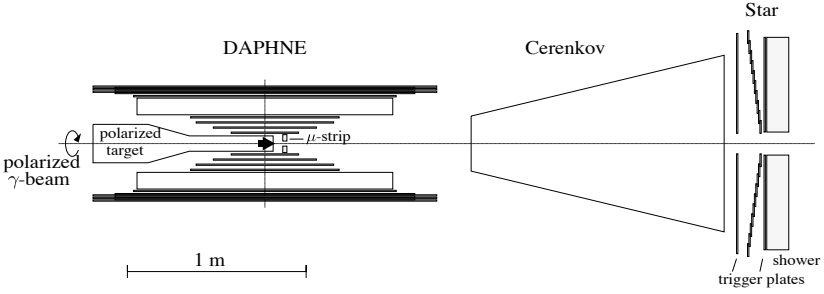

Figure 15 Layout of the detector components for the Mainz measurement of the GDH sum rule including the horizontal dilution refrigerator.

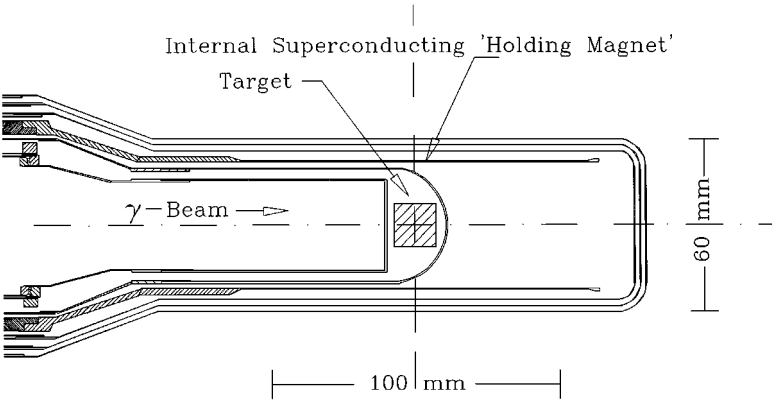

Figure 16 Position of the polarized target within the internal superconducting 'holding magnet' at the downstream end of the ^{3}He/^{4}He dilution refrigerator.

be placed around the ^{3}He/^{4}He refrigerator corresponding to the polarizing or frozen spin (data taking) mode. The spin direction in the frozen spin mode is maintained by a small superconducting magnet placed inside the ^{3}He/^{4}He dilution refrigerator, as shown in Figure 16.

The total thickness of the solenoid coil is about 500 μm including the copper carrier, and its field homogeniety is better than 10^{-3} over the target area. This uniformity allows monitoring of the target polarization in the frozen spin mode, too (84). In the $\bar{p}p \rightarrow \bar{\Lambda}\Lambda$ experiment at LEAR (CERN), where the target material mass thickness of 0.8 g/cm^2 was only increased by 5% by the surrounding walls and liquid He-content (Reicherz G, et al, private communication), the wall thicknesses, traversed by the outgoing particles, were also minimized. Details about the individual components of the experiment are discussed in Reference (111).

GDH measurements with similar target equipment are also proposed at TJNAF and SPRING8 to extend the available energy range up to 5 GeV. Planned GDH experiments at LEGS (90) and GRAAL (91) will use brute force polarized HD targets.

5.3 *Deep Inelastic Scattering and the Spin Structure of the Nucleon*

Deep inelastic scattering (DIS) of polarized leptons from polarized nucleons probes the polarization of the quarks inside the nucleon and, from a knowledge of the interaction of the mediating virtual photon with the nucleon, gives a measure of the contribution of the quarks' spin to that of the nucleon. The measurement of the spin-dependent structure function g_1 for both proton and

neutron allows a test of the Bjorken sum rule (112), a fundamental prediction of QCD.

In such experiments, a scattering asymmetry $A_\parallel$ is measured as discussed earlier in Section 3.5, Target Materials. When both the spins of the lepton and nucleon are parallel to the beam direction, the scattering is compared to that when one of the spins is flipped to the antiparallel direction. Then

$$A_\parallel = \frac{1}{P_B P_T f} \frac{N \uparrow\uparrow - N \downarrow\uparrow}{N \uparrow\uparrow + N \downarrow\uparrow}, \qquad 12.$$

where P_T is the target and P_B is the beam polarization. There is also a transverse asymmetry $A_\perp$, which can be measured, and its associated spin structure function g_2 evaluated when the nucleon polarization is normal to the beam direction. $A_\perp$ and g_2 are small.

However, the physics asymmetry of interest is A_1, the virtual-photon nucleon asymmetry, where the virtual photon polarization is connected via the calculable depolarization factor D to the polarization of the incoming lepton. Ignoring a small term involving the transverse asymmetry $A_\perp$, then $A_1 = A_\parallel / D$. The structure function g_1 is written (again ignoring the small transverse asymmetry term) as

$$g_1 = \frac{F_2 A_1}{2x\,(1 + R)}, \qquad 13.$$

where F_2 and R are unpolarized structure functions, and x is the Bjorken kinematic variable.

The first measurements were made at SLAC (E80 & E130) (3, 4) at 5 T and 1 K with a 4 cm long polarized butanol target (113). Because of the need for high statistics, the availability of a high-intensity polarized electron beam made the experiments possible. In fact, the intensity was limited by target performance and the ability of the butanol to withstand radiation damage.

On the other hand, the EMC experiment at CERN (106) did not have a problem with radiation damage since it used a tertiary beam of polarized muons. Because of its low intensity, it was necessary to increase the luminosity by increasing the target length to about a meter and to take data for long periods. The target material was irradiated ammonia (66), used because of its high polarizable nucleon content. The target was cooled by a powerful dilution refrigerator, at that time the largest in the world (31).

The result of the EMC experiment was that almost none of the spin of the nucleon was carried by the quarks, leading to the so-called spin crisis and to the follow-up experiments SMC and E143 described below. In addition, experiments were run to access the neutron spin structure more directly by using ^{3}He gas targets (114).

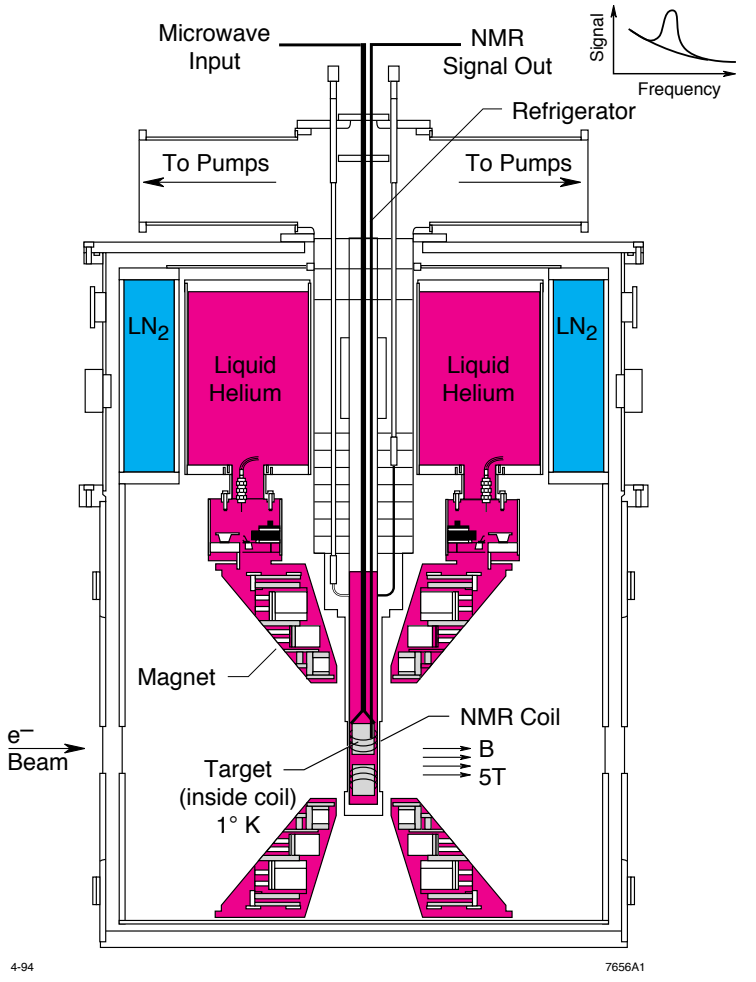

Figure 17 The E143 target and magnet.

5.4 *E143 at SLAC*

With the benefit of improvements in target design and radiation-resistant materials, E143 was able in three months to provide high statistics data on g_1 for the proton, deuteron (and neutron) as well as asymmetry measurements on g_2.

The target used in this experiment is shown in Figure 17 and described in Reference (35). A beam of about $5 \cdot 10^{11}$ electrons per second at 29 GeV was scattered from 3 cm long polarized ammonia targets ($^{15}NH_3$ and $^{15}ND_3$), which resulted in a luminosity of higher than 10^{35}/(sec cm^2). The targets were cooled

by a ^{4}He evaporation refrigerator operating at around 1 K with a cooling power of about 1.5 W in a 5 T field. The proton polarization in $^{14}NH_3$ had previously been shown (7) to have a rapid rise to values over 90%, after preirradiation at 90 K. Tests before E143 showed that this was equally true for $^{15}NH_3$. On the other hand, the deuteron polarization in $^{15}ND_3$ only rose to 13% after the high-temperature irradiation, but a modest additional low-temperature irradiation (discussed in Section 3.5) boosted the achievable polarization finally to $\approx 42\%$, with frequency modulation applied.

The beam was rastered over the face of the target to prevent local depolarization. Typically, after turning the beam on the target, polarization dropped by a few percent over the course of about 10 minutes due to beam heating of the target volume and, then, declined at a lower rate due to radiation damage. After reducing to a given level, the polarization was refreshed by a target annealing, the polarization reversed, and the cycle repeated. A short history of a $^{15}NH_3$ and $^{15}ND_3$ target is shown in Figure 18 (*a*) and (*b*).

In the case of the deuteron, the effect of the low-temperature irradiation pushing the polarization to >40% is apparent. The proton polarization, on the other hand, stays relatively flat. Measurements of the ^{15}N polarizations in both targets and of the residual proton polarizations in the deuteron target were made to correct the asymmetry data. More target details can be found in Reference (35).

Because the electron beam spin direction was flipped randomly on a pulse-by-pulse basis, target polarization did not need to be reversed. However, because of rapid polarization build-up, it was done once or twice a day for consistency checks and for a study of systematic effects. For the same reason a set of data was taken with the magnetic field of the target reversed.

Data on these spin structure measurements have been published by Abe et al (115, 116).

5.5 *SMC at CERN*

The SMC experiment at CERN was the first to access the neutron spin structure and allow a test of the Bjorken sum rule. 190 GeV polarized μ^+ mesons were scattered from polarized protons or deuterons in a very large target; the target material was butanol, or in the final year of running, $^{14}NH_3$. With a beam intensity of $\approx 10^7$ μ/sec, which was more than four orders of magnitude less than at SLAC, the luminosity was increased by having a target two orders of magnitude longer than at SLAC. Even though data were taken for several years, it was not possible to compete statistically with E143. However, the kinematic reach was considerably better than at E143, going to lower Bjorken x values and much higher Q^2.

At first the old EMC target was used, but then an even bigger one was built, cooled by a dilution refrigerator that supplanted the EMC one as the world's

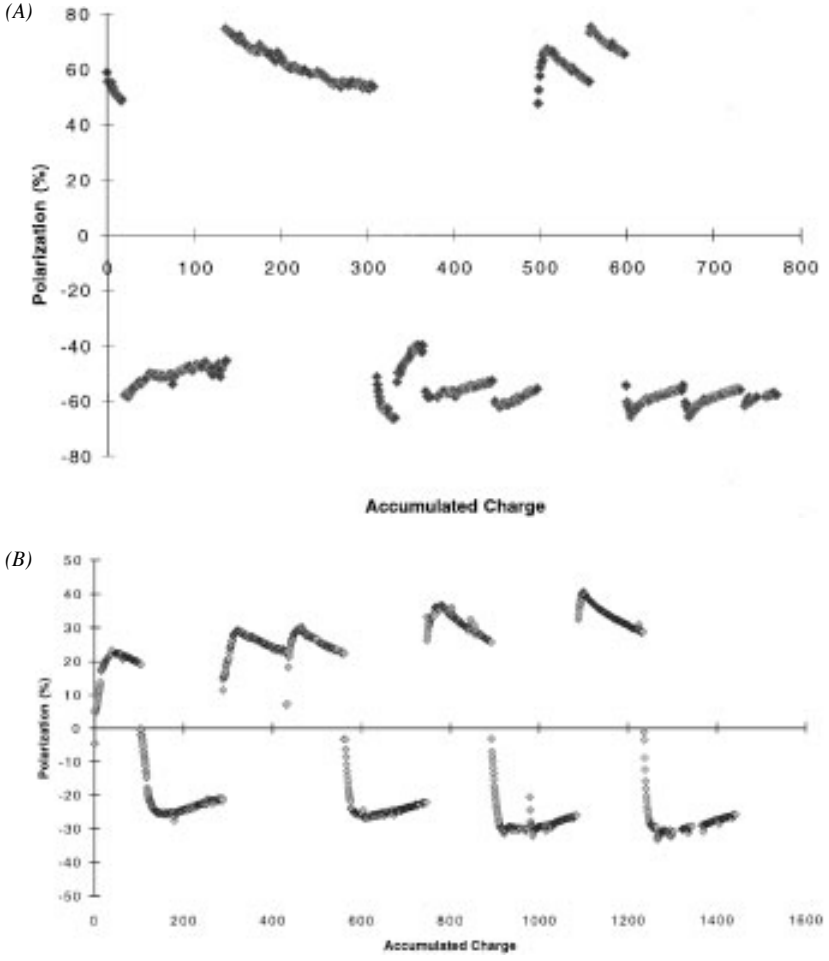

Figure 18 The polarization history of (*A*) protons in $^{15}NH_3$ and (*B*) deuterons in $^{15}ND_3$ as a function of charge on target. One unit of charge is equivalent to 10^{14} electrons.

most powerful. It is shown in Figure 19, connected to a 2.5 T solenoid and is described by Kyynäräinen et al in (33). The mixing chamber was divided into three parts, with two containing the target material, each 60 cm long, and a 30 cm divider the third part. The target sections were polarized in opposite directions and the divider filled with microwave absorber to prevent cross coupling between the sections. A volume of 2.7 l of butanol or $^{14}NH_3$ was required to fill both sections of the mixing chamber. The dilution refrigerator was capable of a cooling power of 1.3 W at 500 mK, yet it could cool to 50 mK, where

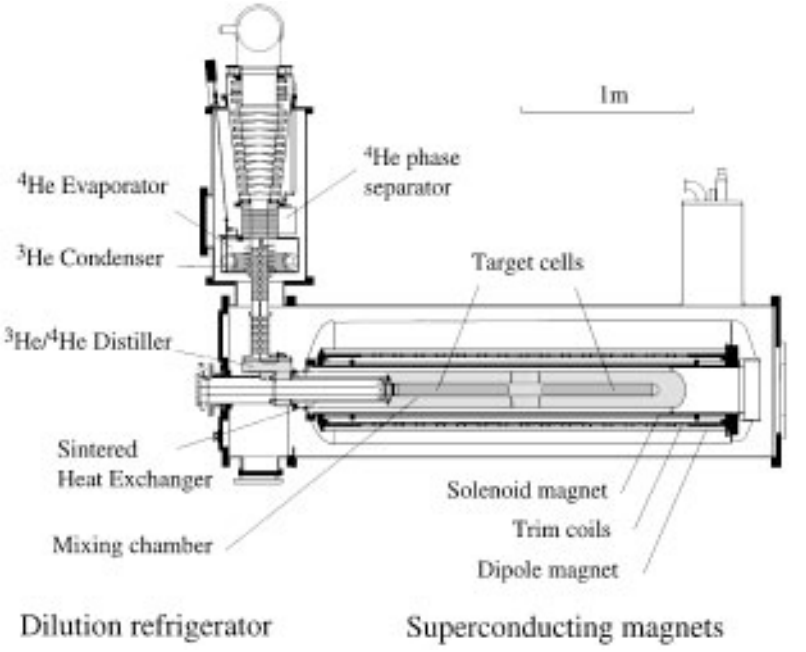

Figure 19 The SMC dilution refrigerator, target, and magnet.

the cooling power was 1 mW for frozen-spin operation. The build-up time for the polarization was several hours, but without any worries of beam heating or radiation damage, polarizing could go on during data taking for several days before saturation occurred. Maximum proton polarizations of $+93\%$ and -94% were obtained in butanol, while average polarization of more than $\pm 90\%$ were reached in $^{14}NH_3$. Typical deuterated butanol polarizations were $\pm 50\%$.

In this experiment, it was not possible to flip the beam polarization (unless one changed to μ^-!) and with a build-up time of hours, it was not very easy to change the target polarization frequently. So a strategy of rotating the solenoid field to the opposite direction was adopted. With 190 GeV muons and a longitudinal field, the effect on the scattered particles was minimal. The field was rotated about every five hours while the target was in frozen spin mode. A dipole was turned on at a strategic time so that the total magnetic field never went below 0.5 T while the solenoid was crossing zero. Each rotation lost only a fraction of 1% of polarization.

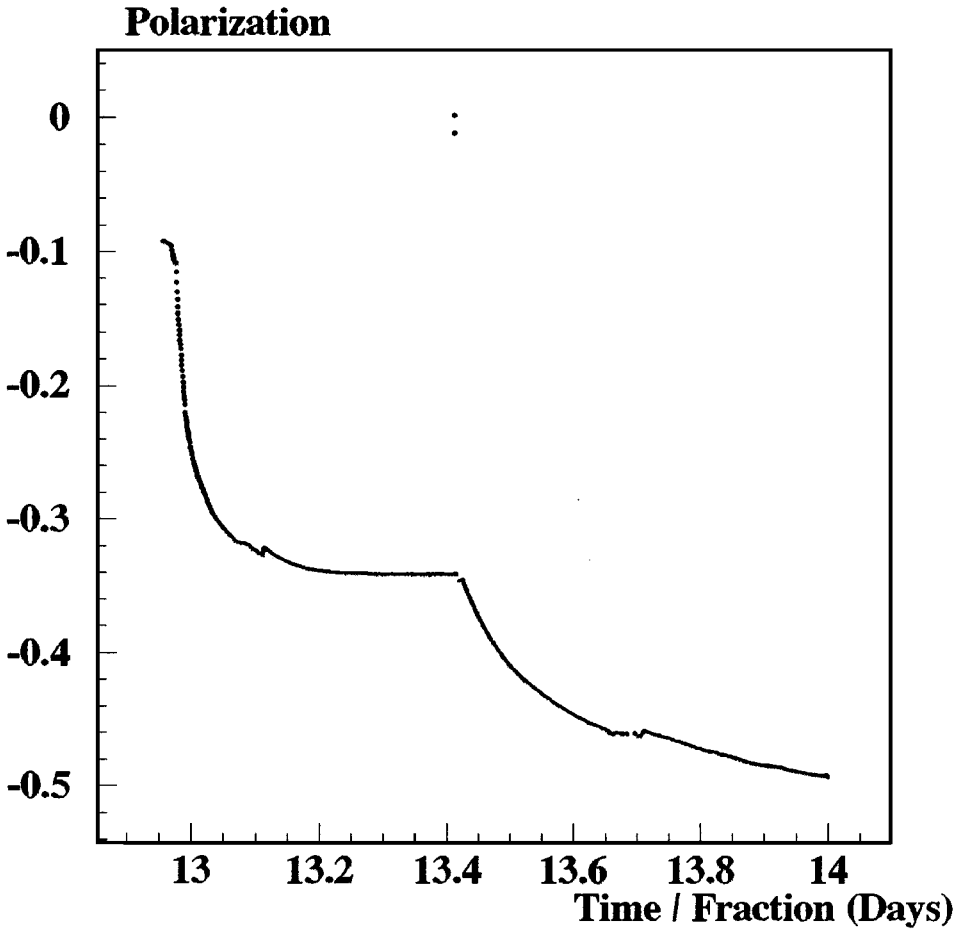

Figure 20 The effect of applying microwave frequency modulation to deuterated butanol. The deuteron polarization first builds up to, and flattens off at ∼34% and then the fm is turned on, driving the polarization up rapidly, finally approaching ∼50%.

During the course of the experiment it was found by Adams et al that frequency modulating the microwaves (117) improved the deuteron polarization by almost a factor of 2 and by about 20% for the proton. The effect for the deuteron is shown in Figure 20.

The data from the latest SMC publications are found in (118, 119); SMC ceased data taking in September 1996, after 5 years. Meanwhile a new experiment at SLAC, E155, has extended the measurements of E143 to 50 GeV after taking data from March 1–April 30, 1997.

6. SUMMARY

The use of solid polarized targets in nuclear and particle physics experiments since the early 1960s has led to better understanding of the role of spin in many interactions. There is now a wealth of data on polarized hadron-hadron interactions, and in recent years several experiments have shed light on the puzzle of where the spin of the nucleon comes from.The first polarized target and the subsequent developments of all aspects of a polarized target system have opened up new experimental possibilities and allowed a choice of approaches to a particular physics problem.

The parallel development of polarized particle beams has enhanced this ability to study some of the outstanding and fundamental problems of particle physics. The Bjorken sum rule in deep inelastic lepton scattering was formulated in 1966, but it has only very recently been confirmed through experiments of the past five years, using state-of-the-art polarized targets. The new electron machines, with their battery of polarized targets, will ensure that in the next few years a similar assault will be made to test the validity of the Gerasimov-Drell-Hearn sum rule and the relation between these two different physical regimes.

ACKNOWLEDGMENTS

The authors are indebted to Stefan Goertz for all his efforts in preparing the manuscript and are grateful to him for the many discussions we had. We also thank Stephen Bueltmann and Seppo Penttila for discussions and critical reading of the manuscript. This work was supported by the US Department of Energy under Grant No. DEFGO2 - 96ER40950, by the Institute for Nuclear and Particle Physics and an AEP grant at the University of Virginia, and by funds from the Bundesministerium für Bildung, Wissenschaft, Forschung und Technologie.

Literature Cited

1. Abragam A, et al. *Phys. Lett.* 2:310 (1962)
2. Chamberlain O, et al. *Phys. Lett.* 7:293 (1963)
3. Alguard MJ, et al. *Phys. Rev. Lett.* 37: 1258 (1976); 37:1261 (1976)
4. Baum G, et al. *Phys. Rev. Lett.* 51:1135 (1983)
5. Antille J, et al. *Nucl. Phys.* B185:1 (1981)
6. Cameron PR, et al. *Phys. Rev.* D32:3070 (1985)
7. Crabb DG, et al. *Phys. Rev. Lett.* 65:3241 (1990)
8. Crabb DG, et al. *Phys. Rev. Lett.* 64:2627 (1990); Crabb DG. *Proc. 9th Int. Symp. on High-Energy Spin Phys., Bonn* 2:289-300. Springer-Verlag (1990)
9. Crabb DG, et al. *Phys. Rev. Lett.* 41:1257 (1978); O'Fallon JR, et al. *Phys Rev. Lett.* 39:733 (1977)
10. Gehring R, et al. *Ein Neuartiges Frozen*

Spin Target zur Messung der Targetasymmetrie in der Eta-Photoproduction an Elsa PhD thesis. University of Bonn, Bonn-IR-97 (1997)
11. Overhauser A. *Phys. Rev.* 92:411 (1953)
12. Abragam A & Proctor WJ. *Compt. Rend. Acad. Sci.* 246:2253 (1958)
13. Jeffries CD. *Phys. Rev.* 106:164 (1957)
14. Jeffries CD. *Phys. Rev.* 117:1056 (1960)
15. Abragam A. *Principles of Nuclear Magnetism*. Oxford: Clarenden (1961)
16. Schmugge TJ, Jeffries CD. *Phys. Rev. Lett.* 9:268 (1962)
17. Borghini M. *Proc. 2nd Int. Conf. Polar. Targets*, ed. G Shapiro, p.1. (1971)
18. Abragam A. *Proc. High-Energy Phys. with Polar. Targets & Beams* AIP Conf. Proc. 51:1 (1978)
19. Jeffries CD. *Proc. 9th Int. Symp. High-Energy Spin Phys.*, eds. W Meyer, KH Althoff. Vol. 1:3 Germany: Springer Verlag (1991)
20. de Boer W. *Dynamic Orientation Nuclei Low Temp*. CERN Yellow Report 74-11 (1974); *J. of Low-Temp. Phys.* 22:185 (1976)
21. Adeva B, et al. In press
22. Borghini M. *Phys. Rev. Lett.* 20:419 (1968)
23. de Boer W, Niinikoski TO. *J. of Low-Temp. Phys.* 114:495 (1974)
24. Baum G, et al. *A Proposal for a Common Muon and Proton Apparatus for Structure and Spectroscopy*, CERN/SPSLC/96-14 (1996)
25. Jeffries CD. *Cryogenics* 3:41 (1963); Abragam A. *Cryogenics* 3:42 (1963)
26. Button-Shafer J. *Proc. Conf. on High-Energy Phys. Polar. Targets & Beams*, ed. GH Thomas, AIP Conf. Proc. 51, p. 41. New York: AIP (1979)
27. Sowinski J, Knutson LD. *Phys. Rev. B* 37:9208 (1988)
28. Borghini M, et al. *Nucl Instr. & Meth.* 49:248 (1967); 49:259 (1967)
29. Herr H, Kadansky V. *Nucl. Instr. & Meth.* 204:59 (1974)
30. Lounasmaa OV. *Exper. Prin. Meth. Below 1 K*. London, New York: Academic (1974)
31. Niinikoski TO. *Nucl. Instr. & Meth.* 192:151 (1982)
32. Niinikoski TO. *Nucl. Instr. & Meth.* 134:219 (1976)
33. Kyynäräinen J, et al. *Nucl. Instr. & Meth.* A 356:47 (1995)
34. van den Brandt B, et al. *Nucl. Instr. & Meth.* A289:526 (1990)
35. Crabb DG, Day D, et al. *Nucl. Instr. & Meth.* A356:9 (1995)
36. SMC Collaboration. *Nucl. Instr. & Meth.* A372: 339 (1996)
37. Goldman M. *J. Magn. Reson.* 17:393 (1975)
38. Court GR, et al. *Nucl. Instr. & Meth.* A324:433 (1993)
39. Niinikoski TO, et al. *Nucl. Instr. & Meth.* A356:62 (1995)
40. Reicherz G, et al. *Nucl. Instr. & Meth.* A356:74 (1995)
41. Krämer D, et al. *Nucl. Instr. & Meth.* A356:79 (1995)
42. Sermertzidis YK, et al. *Nucl. Instr. & Meth.* A356:249 (1995)
43. Dhawan SK, et al. *IEEE Trans. Nucl. Sci.* 43:2115 (1996)
44. Wait GD, Delheij PP, Healey DC. *Nucl. Instr. & Meth.* A274:516 (1989)
45. Kisselev Yu, et al. *Nucl. Instr. & Meth.* A354:249 (1995)
46. Kadansky V. *Photoproduktion negativer Pionen an einem polarisierten Neutronentarget*, PhD. thesis. University of Bonn. BONN-IR-75-54 (1975)
47. Ashkin J, et al. *Proc. Ann Arbor Wkshp Polar. Beams, Ann Arbor, Michigan* p. 42. (1977)
48. Hill DA, Hill JJ. *Argonne Natl. Lab. Rep.* ANL-HEP-PR-81-05 (1981)
49. Krumpolc M, Rocek J. *J. Am. Chem. Soc.* 100:145 (1978)
50. Krumpolc M, et al. *Proc 9th Int. Symp. High-Energy Spin Phys., Bonn, Germany* 2:340 Bonn:Springer-Verlag (1990)
51. Mango S, et al. *Nucl. Instr. & Meth.* 72:45 (1969)
52. Bültmann S, et al. *Nucl. Instr. & Meth.* A356:102 (1995)
53. Hill DA, Crabb DG, Krumpolc M. *Argonne Natl. Lab. Rep.* ANL-HEP-TR-93-15 (1993)
54. Hill DA. et al. *Proc.4th Int. Wkshp Polar.Target Mat. Tech.*, ed. W Meyer, p. 84. Bonn: University of Bonn (1984)
55. Ball J, et al. *Nucl. Instr. & Meth.* A381:4 (1996)
56. van den Brandt B, et al. *Nucl. Instr. & Meth.* A356:36 (1995)
57. van den Brandt B, et al. *Nucl. Instr. & Meth.* 1381:219 (1996)
58. Kageya T, et al. *Proc. 12th Int. Symp. High-Energy Spin Phys., Amsterdam, 1996*, p. 380
59. Rozantsev EG. *Free Nitroxyl Radicals* New York: Plenum (1970)
60. Bunyatowa EI. *Proc. Int. Symp. High-Energy Spin Phys.*, Vol. 2:333. eds. W Meyer, E Steffens Thiel. Germany: Springer Verlag (1991)
61. Niinikoski TO, Rieubland JM. *Phys. Lett.* 72A:141 (1979)

62. Härtel U, et al. *Proc. Int. Symp. High-Energy Phys. Polar. Beams & Targets*, eds. C Joseph, J Soffer, p. 451. Basel: Birkhäuser (1981)
63. Seely M, et al. *Proc. Int. Symp. High-Energy Phys. Polar. Beams & Targets*, eds. C Joseph, J Soffer, p. 453. Basel: Birkhäuser (1981)
64. Althoff KH, et al. *Proc. 4th Wkshp Polar. Target Mat.Tech.*, ed. W Meyer, p. 23. Bonn: University of Bonn (1984)
65. Crabb DG. *Proc. 9th Int. Symp. High-Energy Spin Phys.*, Vol. 2:289, eds. W Meyer, E Steffens Thiel. Germany: Springer Verlag (1991)
66. Brown S, et al. *Proc. 4th Wkshp Polar. Target Mat.Tech.*, ed. W Meyer, p. 66. Bonn: University of Bonn (1984)
67. Meyer W, et al. *Nucl. Instr. & Meth.* 215:65 (1984)
68. Meyer W, et al. *Nucl. Instr. & Meth.* 227:35 (1984)
69. Meyer W, et al. *Nucl. Instr. & Meth.* A244:574 (1986)
70. Roinel Y, et al. *Journal de Physique* 39:1097 (1978)
71. Abragam A, et al. *Phys. Lett.* 41:309 (1980)
72. Bouffard V, et al. *Rev. Phys. Appl.* 13:304 (1978)
73. Chaumette P, et al. *Proc. 8th Int. Symp. High-Energy Spin Phys.*, ed. KJ Heller. Am. Inst. of Phys., No. 187, Vol. 2, p. 1275 (1988)
74. Goertz St, et al. *Nucl. Instr. & Meth.* A356:20 (1995)
75. Schellingerhout NW, et al. *Phys. Rev. C* 48:2714 (1993)
76. *SLAC Experiment E155*. In press
77. Bernard R, et al. *Nucl. Instr. & Meth.* A249:176 (1986)
78. van den Brandt B, et al. *Nucl. Instr. & Meth.* A356:53 (1995)
79. Dutz H, et al. *Nucl. Phys. A* 601:319 (1996)
80. Dutz H, et al. *Nucl. Intr. & Meth.* A340:272 (1994)
81. Lehar F, et al. *Nucl. Instr. & Meth.* A356:58 (1995)
82. Delheij PPJ, Sekachev I. *Nucl. Instr. & Meth.* A356:56 (1995)
83. Ishimoto S, et al. *Jap. J. of Appl. Phys.* 28-10:1963 (1989)
84. Dutz H, et al. *Nucl. Instr. & Meth.* A356:111 (1995)
85. Kisselev Yu, et al. *Mod. Phys. Lett.* B1:409 (1988)
86. Barzhanov NA, et al. *Sov. Phys. Solid State* 31(2) (1989)
87. Reichertz LA, et al. *Nucl. Instr. & Meth.* A340:278 (1994)
88. Honig A. *Phys. Rev. Lett.* 19:1009 (1967)
89. Honig A, Mano H. *Phys. Rev. B* 14:1858 (1976)
90. Babusci D, et al. *Proc. 11th Int. Symp. High-Energy Spin Phys.* AIP Conf. Proc. 343, p. 523. (1995)
91. Didelez JP. *Nucl. Phys. New Europe* 4:10 (1994)
92. *8th Int. Symp. High-Energy Spin Phys.*, ed. KJ Heller. AIP Conf. Proc. No. 187 (1988)
93. *Proc. of 9th Int. Symp. on High Energy Spin Physics*, eds. KH Althoff, W Meyer, Vol. 1. Germany: Springer Verlag (1991)
94. *Proc. of 10th Int. Symp. High-Energy Spin Phys.*, eds. T Hasegawa, et al. Tokyo: Universal Academic (1993)
95. *Proc. 11th Int. Symp. High-Energy Spin Phys.*, eds. KJ Heller, SL Smith. AIP Conf. No. 343 (1994)
96. Stephenson EJ, Vigdor SE. *8th Int. Symp. on Pol. Phenom. Nucl. Phys.* AIP Conf. Proc. No. 339 (1994)
97. Krämer D. *Messung der Targetasymmetrie in der Photoproduktion positiver Pionen mit dem Bonner Frozen Spin Target*, PhD. thesis. University of Bonn, BONN-IR-93-48 (1993)
98. Anton G, Krusche B. *Few-Body Sys.* Suppl. 99:1 Germany: Springer Verlag (1995)
99. Bock A, et al. In press
100. Gerasimov SB. *Sov. J. Nucl. Phys.* 2:430 (1996)
101. Drell SD, Hearn AC. *Phys. Rev. Lett.* 16:908 (1966)
102. Karliner I. *Phys. Rev. D* 7:2717 (1973)
103. Sober DI, et al. *Helicity Struc. Pion Photoproduc.*, CEBAF-PR-91-015 (1991)
104. Ahrens J, et al. *Helicity Depend. Single Pion Photoproduct. Proton*, MAMI Proposal, University of Mainz A2/2-95 (1995)
105. Anselmino M, Joffe BL, Leader E. *Sov. J. Nucl. Phys.* 49:136 (1989)
106. Ashman MJ, et al. *Phys. Lett.* B206:364 (1988)
107. Düren M. *Proc. 31st Recontres de Moriond QCD High-Energy Hadronic Interact.*, ed. J Tran Thanh Van. Les Arcs/F:441 (1996)
108. Burkert V, Li Z. *Phys. Rev. D* 47:46 (1993)
109. Burkert V, et al. *Meas. Polar.Struct.-Func.Inelastic Elect. Scattering Using CLAS*, CEBAF Proposal PR-91-023 (1991)
110. Abe K, et al. *Phys. Rev. Lett.* In press

111. Ahrens J, et al. *Exper. Chk of Gerasimov-Drell-Hearn Sum Rule*, MAMI Proposal, University of Mainz A2/2-93 (1993)
112. Bjorken BJ. *Phys. Rev.* 148:1467 (1966); *Phys. Rev. D* 1:1376 (1970)
113. Ash W. *Nucl. Inst. & Meth.* 134:9 (1976); Seely ML. *Dynamic Nucl. Poalr. Irradiated Target Mat.* PhD thesis. Yale University (1982)
114. Chupp TE. *Ann. Rev. Nucl. Part. Sci* 45:373 (1994)
115. Abe K. *Phys. Rev. Lett.* 75: 25 (1995)
116. Abe K. *Phys. Lett. B* 364 (1995)
117. Adams D, et al. *Phys. Lett. B* 357:248 (1995)
118. Adeva B, et al. *Phys. Lett. B* 329:399 (1994)
119. Adams D, et al. *Phys. Lett. B* 396:338 (1997)

Annual Review of Nuclear and Particle Science
Volume 47, 1997

CONTENTS